Selective Rab11 transport and the intrinsic regenerative ability of CNS axons

Selective Rab11 transport and the intrinsic regenerative ability of CNS axons.

Hiroaki Koseki[1,2], Matteo Donegá[2], Brian Y.H. Lam[4], Veselina Petrova[1,2], Susan van Erp[5], Giles S.H. Yeo[4], Jessica C.F. Kwok[1,2,3,6], Charles ffrench-Constant[5], Richard Eva[1,2,*], James W. Fawcett[1,2,6,*]

1. John van Geest Centre for Brain Repair, University of Cambridge, Robinson Way, Cambridge CB2 0PY, UK

2. Department of Clinical Neurosciences, University of Cambridge, Cambridge CB2 0QQ, UK

3. School of Biomedical Sciences, Faculty of Biological Sciences, University of Leeds, Leeds LS2 9JT, UK

4. Metabolic Research Laboratories and MRC Metabolic Diseases Unit, University of Cambridge, Addenbrooke's Hospital, Cambridge CB2 0QQ, UK

5. MRC Centre of Regenerative Medicine, University of Edinburgh, 5 Little France Drive, Edinburgh, EH16 4UU UK

6. Centre of Reconstructive Neuroscience, Institute of Experimental Medicine, Czech Academy of Sciences, Prague, Czech Republic.

* Co-corresponding authors.

Correspondence

James Fawcett
Brain Repair Centre
Robinson Way
Cambridge CB2 0PY, UK
Email jf108@cam.ac.uk, Tel +441223331160, Fax +441223331174

Short Title: Rab11 and CNS axon regeneration.

Keywords: axon, growth cone, regeneration, axotomy, axon growth, trafficking, axonal transport, endosomes, small GTPases, Rabs, integrin, RNA sequencing.

Summary

Neurons lose intrinsic axon regenerative ability with maturation, but the mechanism remains unclear. Using an *in-vitro* laser axotomy model, we show a progressive decline in the ability of cut CNS axons to form a new growth cone and then elongate. Failure of regeneration was associated with increased retraction after axotomy. Transportation into axons becomes selective with maturation; we hypothesized that selective exclusion of molecules needed for growth may contribute to regeneration decline. With neuronal maturity Rab11 vesicles (which carry many molecules involved in axon growth) became selectively targeted to the somatodendritic compartment and excluded from axons. Their transport changed from bidirectional to retrograde. However, on overexpression Rab11 was mistrafficked into proximal axons, and these axons showed less retraction and enhanced regeneration after axotomy. These results suggest that the decline of intrinsic axon regenerative ability is associated with selective exclusion of key molecules, and that manipulation of transport can enhance regeneration.

Introduction

Axon regeneration fails in the adult mammalian CNS due to a combination of extrinsic inhibitory cues and an inadequate intrinsic regenerative response (Fawcett et al., 2012; Liu et al., 2011). Long-distance regeneration can only be achieved if axons have a high intrinsic growth ability (Liu et al., 2010; Cheah et al., 2016). Embryonic axons have this ability, and can elongate for long distances if immature neurons are transplanted into the adult CNS environment (Lu et al., 2012; Reier et al., 1986). However with maturation, adult CNS neurons lose much of this intrinsic regeneration ability, and axons such as those of the corticospinal tract show limited growth even in a permissive environment such as a peripheral nerve graft (Bradke et al., 2012; Geoffroy et al., 2016)(Richardson et al., 1984). Several changes occur during neuronal differentiation that might explain this maturational reduction in growth ability. Amongst these a key factor that changes radically with maturity is the establishment of selective transport to axons and dendrites (Bentley and Banker, 2016; Britt et al., 2016; Franssen et al., 2015; Maeder et al., 2014; Petersen et al., 2014). Polarised transport of proteins is required for the correct molecules to travel to pre-and postsynaptic sites and in order for axons and dendrites to possess different structures and functions (Britt et al., 2016; Maeder et al., 2014). A consequence of polarised transport is that several key growth-related molecules including integrins, trkB and IGF receptor become excluded from

cortical axons as they mature (Andrews et al., 2016; Franssen et al., 2015; Hollis et al., 2009a; Hollis et al., 2009b). This development of polarised transport therefore provides a possible mechanism for the maturational loss of intrinsic regeneration ability. Our previous work has focused on integrins as an example of a molecule necessary for efficient regeneration and growth (Andrews et al., 2009; Tan et al., 2011; Cheah et al., 2016), and has shown that these receptors are progressively excluded from cortical axons to become exclusively somatodendritic both *in vitro* and *in vivo* (Franssen et al., 2015; Andrews et al., 2016). Conversely, sensory and retinal ganglion cell neurons, which can be more easily manipulated to make them regenerate, continue to transport integrins into their axons into adulthood (Andrews et al., 2016).

Integrins are transported into axons in recycling endosomes marked by the small GTPases Rab11 and ARF6 (Eva et al., 2010; Eva et al., 2012; Franssen et al., 2015). Rab11 is implicated in the trafficking of a number of growth associated molecules, including Trks A and B (Ascaño et al., 2009). Integrins, Trks and Rab11 are all excluded from cortical CNS axons *in-vivo* (Andrews et al., 2016; Hollis et al., 2009; Sheehan et al., 1996). Rab11 is involved in axon elongation in young CNS and adult PNS neurons regenerating *in vitro*, and is required for correct growth cone function as its targeted removal leads to growth cone collapse (van Bergeijk et al., 2015; Eva et al., 2010). These findings led us to ask whether selective exclusion from axons of the Rab11 vesicles that transport these growth-related molecules contributes to their maturational loss of intrinsic regenerative ability, and whether replenishment and/or modulation of activation of Rab11 can enable regeneration.

Previous studies of selective transport have used an *in vitro* model in which cortical neurons mature and exclude integrins from their axons (Franssen et al., 2015; Petersen et al., 2014). We further developed this culture model for regeneration studies, and demonstrated that axons in these cultures lose the ability to regenerate with maturity, and that this loss is intrinsic to the axons rather than due to environment. We found that the characteristics of retraction bulb formation define the probability of regenerating a growth cone, but that subsequent axon elongation is controlled differently. The behaviour of Rab11 was then investigated: we find that it becomes excluded from axons as neurons mature *in-vitro*, but that restoring the presence of Rab11 in axons modifies retraction and enhances regeneration of mature axons.

Results

Cortical neurons mature in the *in-vitro* culture model.

Embryonic CNS neurons can differentiate in culture and provide a model for maturation-related changes (Barbati et al., 2013). We asked whether this type of culture could also be used to model the developmental loss of intrinsic regenerative capacity. Dissociated embryonic day 18 (E18) rat cortical neurons were grown in the presence of astrocyte feeder cultures (Kaech and Banker, 2006). Neuronal maturity was tracked by examining the electrical properties of neurons, their pattern of gene expression through mRNA sequencing, and immunolabelling of cytoskeletal maturity markers. Electrophysiological maturation was examined by patch clamping neurons at 4, 8, 16, and 24 days *in vitro* (DIV) (Fig. 1, Fig 1-figure supplement 1). During time in culture, resting membrane potential lowered to -55mV (Fig. 1A) and membrane capacitance increased (Fig. 1B). Only 29.4% ± 10.6% of neurons were able to fire action potentials in response to steps of depolarizing current at 4 DIV, but the percentage increased to 100 % by 24 DIV (Fig. 1C,E). Concurrently the action potential spikes turned from single to multiple (Fig. 1E), increased in amplitude (Fig 1 figure supplement 1A), decreased in duration (Fig. 1 figure supplement 1B) and spike threshold increased (Fig. 1 figure supplement 1D) while input resistance decreased (Fig. 1 figure supplement 1E). All of these are changes associated with the maturation of neurons *in vivo.* Interestingly, the main statistical difference for these parameters was observed between 8 DIV and 16 DIV. As for network development, compatible with a previous study (Kay et al., 2011), co-localization of both excitatory and inhibitory synaptic markers was observable by 10DIV (Fig. 1 figure supplement 1F). However, spontaneous activity increased between 16 DIV and 24 DIV (Fig. 1D).

RNA sequencing showed progressive changes in many genes towards expression patterns typical of mature neurons. From the mRNA expression data we picked two useful maturity markers which are cytoskeletal-related molecules and show robust immunostaining: doublecortin and low molecular weight neurofilament. Immunostaining showed a decrease in doublecortin and an increase in low molecular weight neurofilament with neuronal maturation similar to the changes in their mRNA levels (Fig. 1 figure supplement 2A, B, C). Ingenuity pathway analysis of genes with increasing expression showed many changes in molecules involved in synapse formation (Fig.1 figure supplement 2D), whereas many of the

genes with decreasing expression were involved in neuronal development (Fig. 1 figure supplement 2E). Full results are available on NCBI GEO DataSets (RRID:SCR_005012, accession no: GSE92856). Neurons started to develop axon initial segments visualized by immunostaining for neurofascin and Ankyrin-G as early as 3 DIV, and the structure consolidated with increasing DIV (Fig. 1 figure supplement 3A). There was little neuronal loss in the cultures up to DIV24, and neurons showed no cleaved caspase 3 expression after 3 weeks in culture (Fig. 1 figure supplement 3B, C). These results demonstrate that neurons in this culture model show maturational changes similar to those of neurons *in vivo* and remain viable.

Characterization of the axotomy response of rat cortical neurons

In vitro laser axotomy was performed at 4, 16 and 24 DIV and the events that follow axotomy were recorded. To distinguish individual axons from the large number of surrounding processes, small numbers of neurons were transfected with GFP and before axotomy fluorescent live neurofascin staining of the axon initial segment (AIS) was used in all cases to identify axons from dendrites (Fig 1 figure supplement 3A). Events after axotomy unfold over several hours for CNS axons (compared with sensory axons which usually regenerate within one hour). Cultures were therefore filmed using time-lapse microscopy for 10~20 hours. Axotomy was followed by either neuronal death, branch loss or retraction bulb formation (Fig. 2A,B). Neurons were considered dead if axon disintegration or cell disruption was seen within 10hrs of axotomy, and were excluded from further analysis: this occurred in 15~25% of axotomies with no variation with DIV (Fig. 2B,C). Branch loss was the retraction of the cut axon branch to the nearest branch point with no formation of a retraction bulb: this occurred in 10~15% of axotomies (Fig. 2B,C) which were also excluded from further analysis. Retraction bulb formation was the commonest result of axotomy. Starting immediately after axotomy, the GFP signal within the axon disappeared proximal to the cut for up to 1000 µm. Following this, the cytosol would reflux up to the newly sealed axon tip and start accumulating to form a retraction bulb which was usually motile; this usually took from 1 to 3 hours (see below) (Fig. 2 A,C). The appearance of the retraction bulb under fluorescence imaging and phase contrast were identical.

After successful formation of a retraction bulb three outcomes were seen (Fig. 3); regeneration of a new axon from the bulb (usually following a different track) (Fig. 3A,B), failure of regeneration (although the retraction bulbs were usually motile), or ectopic growth (formation of a new axon branch from the side of the cut axon, usually within 100 µm of the

bulb) (Fig. 3B). The probability of these events changed radically with neuronal maturity; in 3-5 day old neurons over 70% showed axon regeneration, but by 23-30 days less than 10% regenerated (Fig. 3C). Typical videos of successful regeneration in a DIV4 neuron and failure of regeneration in a DIV30 neuron are shown in (Videos 1 and 2). In the further analysis we have combined the results of regeneration and ectopic growth into an overall regeneration score. To describe regeneration more precisely, we also measured 6 regenerative factors; retraction distance, retraction bulb formation time, regeneration ratio, regeneration initiation time, regeneration length, and growth cone area and these were measured for proximal and distal axotomies. (measures defined in Table 1).

Maturation-related changes in retraction and regeneration.

The dynamics of retraction bulb formation varied considerably with maturity. The retraction distance increased with DIV (Fig. 4, Fig. 4 figure supplement 1A) and the time taken to form a retraction bulb increased from 1.39 ± 0.21 hrs in 4 DIV neurons to 2.68 ± 0.20 hrs in 24 DIV neurons ($p<0.0001$, Fig. 4S1B), correlating with retraction distance (Fig. 4S1C). The retraction distance had a log Gaussian distribution and we used a log10 conversion for statistical analysis, finding an increase and change in distribution between 4 DIV and 24 DIV (log10 4 DIV: 1.65 ± 0.06, 24 DIV: 2.16 ± 0.03, $p<0.0001$, Fig. 4A. The same data are plotted on a non-log scale in Fig4 figure supplement 1A-E). Interestingly a biphasic distribution with long and short retractors could be seen at 16 DIV, suggesting a transition period, and then all 24DIV axons were long retractors. We analysed these long (≧ 70 μm) and short (< 70 μm) retracting neurons separately in our further analysis of retraction distance and regeneration. For retraction distances, in 4 DIV neurons and short retracting 16 DIV neurons the position of axotomy was not a factor; short retracting axons were seen after both proximal and distal axotomy (Fig. 4B). However the in long retracting 16 DIV neurons and all 24 DIV neurons, distal axotomy led to a greater retraction distance on average than proximal axotomy (>600 μm for 16 DIV and >400μm for 24 DIV) (Fig. 4B Fig. 4 figure supplement 1E). We next focused on regeneration. The DIV of neurons had a powerful negative impact on regeneration, with only 8 % of 24 DIV neurons that formed a retraction bulb regenerating compared to 63 % in the 4 DIV group ($p<0.0001$, Fig.3C, 4C). Longer retracting neurons showed a general tendency for less regeneration (Fig.4G), consistent with a previous *in vivo* result (Canty et al., 2013). Therefore, we categorized axons according to short or long retraction, and by proximal or distal axotomy (Fig. 4C). Distal axotomy led to

less regeneration in the long retraction group of 16 DIV neurons (proximal 64 % vs distal 11 %, p=0.0002) and in 24 DIV neurons which all showed long retraction (proximal 24 % vs distal 2 %, p=0.0116), but distal axotomy did not affect regeneration success in the short retraction groups (p=0.0325) (Fig. 4C). In summary, with increasing DIV retraction distance increased and so did regeneration failure, particularly in axons that showed long retraction and after distal axotomy.

We examined other growth cone behaviour measurements related to regeneration, including regeneration initiation time which increased with DIV and growth cone area which declined (Fig. 4 D,F). The length of the regenerated axon 2 hrs after regeneration initiation also declined with DIV (Fig. 4E). These factors mainly changed between 4 and 16 DIV, and within the 16 DIV axons, retraction and axotomy distance did not influence these measures (Fig. 4S1 F,G,H). Taken together, it can be concluded that 1) long retraction is prognostic for poorer regeneration initiation, and 2) the neuron's ability to successfully initiate regeneration does not dictate how rapidly the axon will then elongate.

The maturing environment of the culture is not inhibitory to regeneration.

Having established a model which shows regenerative decline with DIV, we asked whether this was due to a build-up of inhibition in the culture environment or to an intrinsic loss of regeneration ability in the axons. To address this, we plated newly harvested immature neurons transfected with GFP onto mature 21 DIV cultures without changing the medium, and allowed them to grow for 4 days, resulting in a 4 DIV neuron surrounded by a 25 DIV environment (Fig. 5). Interestingly, 4 DIV neurons on 25 DIV cultures had longer and more complex axons than 4 DIV neurons on PDL (Fig. 5A-C). When axotomized, 4 DIV neurons on 25 DIV cultures behaved very similarly to 4 DIV neurons on PDL, with short retraction (Fig. 5D), and high regeneration success (54 % for 4 DIV neurons on PDL, 46 % for 4 DIV neurons on 25 DIV cultures, and 2 % for 24 DIV neurons, $p<0.0001$, Fig. 5E). These results demonstrate that maturation of the culture environment does not explain the observed regenerative decline with DIV.

Rab11 positive vesicles are excluded from axons in mature neurons.

Having achieved an *in vitro* model in which to study the loss of intrinsic axon regeneration with maturation, we explored potential mechanisms. Based on our previous work, our hypothesis was based on the selective axon transportation that develops with maturity, directing some molecules to dendrites others to axons. We asked whether this process leads

to exclusion of molecules from the axon that are necessary for regeneration. We focused on Rab11 because it is associated with the major recycling endosomes responsible for bringing growth receptors and integrins into axons, and because these endosomes are reported to be restricted to a somatodendritic distribution *in-vivo* (Sheehan et al. 1996, Eva et al. 2010, 2012). The distribution of endogenous Rab11 was studied by immunostaining, which revealed that at 4 DIV Rab11 is present equally in both axons and dendrites, but becomes exclusively somatodendritic by 16 DIV (axon stem/dendrite ratio: 4 DIV 2.05 ± 0.21, 16 DIV 0.23 ± 0.03, p=0.0001, Fig. 6A,B). The immunofluorescence intensity of Rab11 in the cell bodies did not change between DIVs (Fig. 6C), and neither did the mRNA level (Fig. 1 figure supplement 2F), whereas the axon stem/cell body ratio decreased and dendrite/cell body ratio increased between 4 DIV and 16 DIV (Fig. 4B,D). Collectively these results show that Rab11 becomes progressively excluded from axons but not dendrites as neurons mature.

In order to understand the transport dynamics that lead to the selective distribution of Rab11, we examined Rab11 trafficking in axons and dendrites at 16 DIV using transfection of GFP-tagged Rab11a. Previous studies have demonstrated different trafficking mechanisms for the active and inactive forms of Rab11 (Welz et al., 2014), so tagged wild type (WT), dominant negative (DN), and constitutively active (CA) forms of Rab11a were transfected. Overexpression of all forms caused a degree of mis-trafficking in neurons, leading to some Rab11 being found in proximal axons and an increase in the proximal axon/dendrite ratio for total Rab11 (GFP 0.62 ± 0.05, WT 0.63 ± 0.04, DN 0.61 ± 0.04, CA 0.51 ± 0.05, Fig. 7A,B). However, the quantity declined rapidly with distance from the cell body and the transfected Rab11a failed to reach distal axons compared to GFP, confirming an active but slightly leaky exclusion mechanism for Rab11a vesicles in axons (Fig. 7C,D). Previously we have shown that integrin-containing vesicles move mostly retrogradely in mature axons (Franssen et al., 2015), so we examined Rab11a vesicle movements using time lapse imaging, illustrated in kymographs. Similar to integrins, there was a predominance of retrograde movement in 16 DIV axons, and little anterograde vesicle movement. In dendrites, however movement was equal in both directions (Fig. 7E,F). Predominantly retrograde transport in axons was seen for all Rab11 forms, most prominently with the DN (Fig. 7F). The average vesicle velocity for both anterograde and retrograde movement was also slower in axons for WT and CA compared to dendrites (Fig. 7 figure supplement 1A,B). Taken together, these results show that Rab11 becomes selectively excluded from axons by 16 DIV, and that the overall direction of Rab11a transport prioritizes exclusion from axons and transport into dendrites by 16 DIV.

Overexpression of Rab11a enhances regeneration.

As shown above, newly plated neurons show robust rapid axon growth and a high proportion of them regenerate after axotomy. Since this matches the period when axonal Rab11 is still abundant, we asked if axons could regain their regenerative state if Rab11 was returned to the axon at 16 DIV. In principle this should enable transport of many growth-related molecules into the mature axon. Taking advantage of mis-trafficking after overexpression to re-introduce Rab11 into axons, we axotomized axons of Rab11a WT, DN and CA transfected neurons in the proximal zone. Staining for total Rab11 in transfected neurons confirmed that transfection had increased total Rab11 in the proximal axons, and the proximal axon/dendrite ratio of immunofluorescence intensity was increased (Fig. 7A,B).

Axons were cut in the proximal region where Rab11 was now present and their regeneration behaviour was measured. Laser axotomy led to an accumulation of fluorescent Rab11a for all forms in the retraction bulb (Fig. 8A, Fig. 8, Video 3), showing that transfected Rab11 is present during the reorganization of the severed stump. Interestingly, in some cases this accumulation started even before (~30 min) the reflux of the cytosolic GFP or bulb formation (Fig. 8A, Video 3). We then analysed the regenerative measures as in the previous experiments. As with GFP-transfected neurons, retraction distance and time to form a retraction bulb was correlated (Fig. 8B), and the retraction distance of Rab11a transfected neurons showed a biphasic distribution for all forms (Fig. 8C), so we again separated neurons into short and long retraction groups. The percentages of axons in the short and long retraction groups did not change between GFP and the other Rab11a forms. But strikingly, for all Rab11a forms, overexpression resulted in decreased retraction in the long retraction group (Fig. 8E). The presence of Rab11a also influenced growth cone regeneration, and the long retraction group of Rab11a neurons had an improved regeneration ratio, but only with the WT and DN form suggesting the importance of the inactivated state of Rab11 (GFP 11%, WT 38%, DN 38%, CA 13%, GFP vs WT $p=0.0174$, GFP vs DN $p=0.0342$, Fig. 8F). No pro-regeneration effect was observed in the short retraction group (Fig. 8F).

For other measures, regeneration initiation time was unchanged (Fig. 8G), but the length of the axons after 2 hrs was increased with Rab11a WT and CA (Fig. 8H). Growth cone area was also enlarged in regenerating neurons transfected with Rab11a WT, and a trend was seen with the CA but did not reach significance (Fig. 8I). In summary, increasing Rab11a in the axons of 16 DIV neurons led to enhancement of regeneration especially in the long retraction

group. The activation state of Rab11a was a significant factor, with the DN form promoting growth cone formation and the CA form stimulating subsequent elongation.

Overexpression of Rab11 enables integrin transport into axons

Our hypothesis was that Rab11 forced into axons by overexpression would carry with it molecules that promote axon regeneration. We therefore transfected neurons with Rab11-GFP or control GFP at DIV10, the time at which partitioning of transport between axons and dendrites becomes apparent. At DIV 16 the neurons were stained for GFP and for a growth-associated receptor normally excluded from mature neurons. For this growth-related molecule normally carried in Rab11 vesicles we selected α5 integrin (Caswell and Norman, 2006; Eva et al., 2010; Gardiner et al., 2007; Hulsbusch et al., 2015), which is present in neurons and can be detected with a reliable antibody. The level of α5 immunostaining was measured by drawing a linear AOI along the axons (identified by staining the AIS with neurofascin) and dendrites and subtracting the same AOI moved to the background. The results were plotted as axon/dendrite intensity ratio (Fig. 9B) and absolute level (Fig.9C). As above, overexpression of Rab11-GFP led to its presence in the axons over approx. the proximal 200μm (Fig.9A). The distribution of α5 integrin changed similarly. In control GFP-transfected neurons α5 integrin was not detectable in axons (Fig. 9A-C), while in Rab11-GFP-transfected neurons the staining intensity was similar between proximal axons and dendrites (Fig. 9A-C). This experiment shows that Rab11 is able to carry growth-related receptors into axons.

Axonal Rab11 function is conserved in human neurons

Next, we investigated whether the relationships between maturation, Rab11 distribution, axonal expression and regeneration are conserved in human neurons, taking advantage of recent advances that have made it possible to generate human dopaminergic neurons *in vitro*. The human embryonic stem cell (hESC) line RC17 (Roslin Cells) was induced to dopaminergic neuronal differentiation using a protocol in which differentiated post-mitotic neurons are generated within day (d)35 after neural induction (Kirkeby et al., 2012), and the cells were then allowed to mature *in vitro* for up to d65. As in the rodent neurons, laser-mediated axotomy revealed a maturation-related loss of capacity for axonal regeneration. Between d35-40, successful axonal regeneration was seen in over 70% of neurons, but this dropped to 46.9% and 39.6% between d45-55 and d55-65 respectively (fig 10A).

To determine whether this maturation-related loss of regenerative capacity was associated with a reduction in Rab11 trafficking into the axon, we expressed Rab11-GFP in the human neurons. At d41, the level of Rab11-GFP fluorescence was similar in axons and dendrites. At d51 and d65 Rab11-GFP was just detectable in the axons but there was a significant drop relative to levels in the dendrites (Fig 10B,C). We asked whether, as in the rodent neurons, Rab11 overexpression could restore the loss of axonal regeneration potential. Transfection of Rab11 did not affect the rate of axonal regeneration in d35-40 neurons, but a significant increase in the number of axons showing regeneration was seen in d45-55 axons (Fig 10A) with an associated increase in the extent of elongation at 2hrs post-axotomy (Fig 7D) These results confirm that, as in rodent neurons, there is an age-dependent loss of axonal regeneration in human CNS neurons that is associated with loss of axonal Rab11.

Discussion

In order to analyse why CNS neurons lose their ability to regenerate with maturity, and to develop regeneration-promoting treatments a manipulable *in vitro* model is needed. We describe an *in-vitro* single neuron axotomy model, in which there is a progressive decline in the intrinsic regeneration ability of the axons of cortical neurons as they mature. The neurons in these cultures can be transfected and regeneration-promoting effects of pharmaceuticals and other interventions tested (unpublished observations). We describe here an analysis which demonstrates that the development of polarised neuronal transport is an important factor in the loss of regeneration ability, through exclusion of Rab11 recycling endosomes (which contain key growth molecules) from axons. The main influence on regeneration in this study was neuronal maturity, represented by days in vitro (DIV). This is in line with many *in vivo* studies which show that the regenerative ability of CNS axons is lost with maturity. Neuronal maturity is also a key factor *in vivo,* where grafted embryonic neurons have shown extensive growth in the adult brain and spinal cord, yet mature neurons show no growth (Jakeman and Reier, 1991; Kim et al., 2006)(Lu et al., 2012). In *C.elegans* axons also lose regenerative ability with age, although the mechanism may be rather different (Tang and Chisholm, 2016; Byrne et al., 2014). Even when regeneration is stimulated by manipulation of signalling pathways using Phosphatase and Tensin Homolog Deleted from Chromosome 10 (PTEN) deletion, the knockdown is much more effective if it is performed during the growth phase of cortical neurons rather than adulthood (Du et al., 2015; Geoffroy et al.,

2016). However some regenerative events are seen after CNS axotomy in adulthood. In the corticospinal tract and other pathways extensive lateral sprouting can occur (Bareyre et al., 2004), particularly in primates (Rosenzweig et al., 2010), and growth into embryonic grafts can occur (Bernstein-Goral and Bregman, 1993; Kadoya et al., 2016).

Detailed quantification of the events following axotomy revealed behaviours that change at different DIV. The retraction distance after axotomy increased with maturity; at 4 DIV retraction distances were short, but by 24 DIV they were much longer, with a mixture of short and long retractors at 16DIV. Retraction distance predicted regeneration with long retractors seldom regenerating, especially after distal axotomy. The correlation between long retraction and regeneration failure has also been shown *in vivo* after cutting intracortical axons by laser (Canty et al., 2013). We suggest that the increased retraction distance with maturity may reflect changes in cytoskeletal dynamics together with decreased anterograde transport of materials required to maintain the axons. At DIV16, where we see both long and short-retracting axons indicating a mixed degree of maturity in neurons as they are becoming polarized and selective transport is being established (Franssen et al., 2015). By DIV 24 these changes are fully established and all axons show long retraction after axotomy and almost complete loss of regenerative ability. The speed of axon growth after initiation of regeneration and the size of regenerated growth cones declined earlier than these retraction changes, the changes being complete by 16 DIV. Growth cone size is affected by many environmental and intrinsic factors, does not correlate with axon growth speed (Harris et al., 1987; Hur et al., 2012; Tosney and Landmesser, 1985), and is probably not a useful general indicator of regenerative ability.

We focused on the hypothesis that the developmental change in regenerative ability in axons is related to the progressive exclusion of growth-related molecules from axons (Bentley and Banker, 2016; Britt et al., 2016). In particular, previous work has shown that integrins (Franssen et al., 2015) and Trks (Hollis et al., 2009) become excluded from axons after they mature, as are most postsynaptic proteins. Precise control of the location of intracellular molecules is necessary so that axons or dendrites can have different structures and functions. Many growth-related molecules are transported into axons via the recycling pathway in vesicles marked by the small GTPase Rab11 (Lasiecka and Winckler, 2011)(Baetz and Goldenring, 2013; Welz et al., 2014). In this study, we show that Rab11 is present in immature axons but becomes restricted to a somatodendritic distribution with maturity, correlating with the loss of ability to regenerate axons in both rodent cortical neurons and

human dopaminergic neurons. As with many molecules the selective transport mechanism is somewhat leaky, which could indicate passive diffusion of vesicles and molecules into axons followed by selective removal by retrograde transport. Overexpression of Rab11 leads to mis-trafficking and therefore leads to the presence of some Rab11 in the proximal axons of mature neurons. This allowed us to ask whether the presence of Rab11 affects regeneration.

In our study, Rab11 WT and CA enhanced regeneration length and growth cone size, and this is in line with previous studies where these molecules have been shown to be involved in axon and dendritic growth (Park et al., 2006). Our results also demonstrated that along with WT the DN mutant enhances formation of a new growth cone to initiate regeneration whereas the CA does not. Other studies have also confirmed the protrusion-initiating properties of Rab11 DN (Shirane and Nakayama, 2006; Ramel et al., 2013), suggesting that the different forms of Rab11 can have different effects on different processes including vesicle transport, trafficking and actin reorganization and can therefore affect different phases of regeneration. Rab11 overexpression also enhanced regeneration in human dopaminergic neurons. The regeneration-promoting effect of Rab11 overexpression is assumed to be due to the transport into axons of the many growth-related molecules that are transported in this class of endosome (Welz et al., 2014). As an example, we showed that α5 integrin is transported into the proximal axons of Rab11 overexpressing neurons.

Rab11 transport is controlled in several ways. A transport complex of Rab11, Arf6 and JIP3/4 can associate with kinesin or dynein depending on the activation state of Arf6 (Montagnac et al., 2009) and Rab11 associates with kinesin through activated protruding (Matsuzaki et al., 2011). Enhancing the level of PIP3 through PTEN knockdown has been a successful method for inducing regeneration (Liu et al. 2010, Du et al. 2015). Our results fit with this story, because PIP3 has effects on transport through GAPs and GEFs and on membrane trafficking (Macia et al., 2008; Randazzo et al., 2001). It is probable that there is a cycle, where transport of receptors allows PI3K activation and PIP3 generation, which in turn enhances transport and trafficking (Cheng et al., 2011). Manipulation of Rab11 transport using these methods can enhance regeneration in mature cortical neurons (Unpublished observations), and will be the basis of future *in vivo* investigations.

The changes in transport that we have shown affect regeneration, but CNS axons nevertheless show some regenerative activity after damage, particularly lateral sprouting and growth into embryonic tissues. It is unlikely that these events can happen without the

presence of a receptor on the axons and a corresponding ligand in the environment. These receptors, currently unidentified, must continue to be transported into mature axons, presumably independently of Rab11.

Overall this study supports the concept that CNS axons lose their intrinsic ability to regenerate with maturation. Mature axons lose regeneration-associated molecules due to the development of polarised transportation, which directs the many growth-related molecules in Rab11 vesicles to dendrites and away from axons. Modifying selective axon transportation could therefore be a strategy for enhancing intrinsic regeneration ability in the adult CNS.

Experimental Procedures

Cell culture

Cortical neurons were derived from E18 Sprague Dawley rat cortex, and were plated at the density of 100-150 cells/mm^2. The medium used for plating was a combination of fresh B27 medium (neurobasal medium supplemented with 2% B27 and 1% Glutamax) and B27 medium conditioned by astrocytes.

Astrocytes were derived from P0-2 Sprague Dawley rat cortex, and were grown for 7-8 days before being frozen for future use. They were then thawed and further grown for another 5-6 days before being combined with neurons as co-culture, or used for B27 medium conditioning. The co-culture method was adapted from a previously established method (Kaech and Banker, 2006).

Plasmid transfection

Neurons were transfected via microporation or magneting transfection. Microporation was done by using the Neon® Transfection System (Invitrogen), following the manufacturer's protocol. Neurons were plated at a higher density of 200-300 cells/mm^2 to compensate for cell death. This method was mainly used for axotomizing at 4 and 24 DIV.

The Magnefect System (Magnefect nano®, nanoTherics) was mainly used on neurons cultured for 13-14 DIV, following the manufacturer's protocol. DNA transfected with this method expressed within 2 DIV, and was mainly used for 16 DIV axotomy experiments which required co-transfection of plasmids.

Cytoplasmic GFP was from Lonza (pmax GFP), and Rab11a WT GFP/mCherry has been described previously (Eva et al., 2010). Rab11a DN RFP/ CA RFP were kindly provided by Dr. Gonzalo Solis (Université de Lausanne).

Live neurofascin staining

Pan neurofascin extracellular antibody was dialyzed overnight by a 12-14kDa dialyzer (D-Tube™ Dialyzer Maxi, MWCO 12-14 kDa/ Millipore) against 1xPBS (594nm wavelength) or 0.1M borate buffer (650nm wavelength). Then the dialyzed antibody was labeled with a 594 (650) nm wave length dye by following the protocol of the DyLightTM 594 Microscale Antibody Labeling Kit (Thermo Fisher). The labeled antibody was added to the culture immediately before the axotomy session at 1:1000, and was not removed.

Laser axotomy

The laser chamber was kept at 37 degrees at all times, and CO2 was set at 10 %. The immunofluorescence exposure was minimized in order to control phototoxicity. Axotomy was performed by an UV Laser (355 nm, DPSL-355/14, Rapp OptoElectronic) connected to a Leica DMI6000B (Leica Systems), and all images were taken with an EMCCD camera (C9100-02, Hamamatsu).

Neurons transfected with cytosolic GFP were axotomized at different DIV (4, 16, 24 DIV) and distance (250-2000 μm) from the cell body. Large neurons with the anatomy of projection neurons, with several dendrites and a single axon were selected. All axons were confirmed by checking the live neurofascin staining, and neurons with more than 2 axons were excluded from the study. Astrocytes were not removed during axotomy.

Axotomy distance was defined as the axon length between the stem of the axon and the laser shot epicenter, which was manually traced and measured using the Leica application suite AF. To minimize the influence of branch points and adjacent branches, axotomy locations were chosen at least beyond the first branch point, and as far away as possible from any visible branch points. All efforts were made to keep the laser power consistent and cutting to a minimum, but priority was given to make a clean cut.

Post laser response was imaged every 20-30 minutes for every axotomized neuron, starting immediately after axotomy. Imaging was continued in many cases more than 15 hours, and the first 10 hours were used for analysis. Axotomy results were pooled into one group, but axotomy sessions which suffered large amounts of death were excluded. All axotomy results were manually analysed using the Leica application suite AF software.

Live imaging for vesicle tracking

All live-cell imaging for Rab11 vesicle movement studies was performed using an Olympus IX70 microscope equipped with a CCD camera (ORCA-ER, Hammamatsu) and a PerkinElmer UltraVIEW scanner for spinning disk confocal microscopy. MetaMorph software was used to operate the system.

Rab11 vesicle movements were imaged at the proximal axon and dendrite; the first 100 μm segment was considered as proximal. Images were taken 1 frame/second for 3 minutes. Kymographs were obtained from the most well focused 30 μm strip of the axon or dendrite. Vesicles moving only in one direction for more than 2 μm were defined as either anterograde (towards the distal axon) or retrograde (towards the cell body). Vesicles moving in both directions over 2 μm was termed as bidirectional. The average speed for every anterograde or retrograde movement during the imaging period was quantified, and their average was reported as the cell's anterograde or retrograde vesicle velocity. All analysis was performed with FIJI.

RNA sequencing

Total RNA was extracted from 1, 4, 8, 16, and 24 DIV cultures by using the Qiagen RNeasy Micro Kit (Qiagen, 74004), following the manufacturer's instruction. 6 samples were used for each time point.

The extracted RNA was quality checked with the Agilent Bioanalyzer Pico Chips (RIN >7.0) and 2 ng was used for whole transcriptome amplification using NuGEN RNAseq System V2 to generate ds-cDNA. Subsequently, 2 ug of amplified cDNA was subjected to library preperation using NuGEN Ovation Multiplex System. This was then sequenced using an Illumina HiSEQ 2500 instrument, which yielded an average of 12.35M single-end 50 bp reads per sample. The reads were then aligned onto the Rattus Norvegicus Rnor 5.0 genome using Tophat (v2.0.8, RRID:SCR_01) with a mapping rate of 91.67%, and used for differential expression analysis using Cufflinks (v.2.2.1 RRID:SCR_014597). Genes were defined as increasing (decreasing) if 1) the highest FPKM value was more than 3 folds of the lowest FPKM, 2) the false discovery rate adjusted p value between the highest and lowest FPKM calculated by Welch's t-test was smaller than 0.05, and 3) at least one of the time points marked a FPKM value of more than 10. Increasing and decreasing genes were subjected to pathway analysis using the Ingenuity pathway analysis program.

Patch clamping

Whole-cell patch-clamp recordings were performed on 4, 8, 16, 24 DIV neurons, and the neurons' passive membrane properties and spike properties were measured. 800 ms long negative and positive currents were applied in an alternating manner, and the currents were increased in 20 pA steps. The results were recorded in current-clamp mode. All spike events that accelerated over 20 mV/ms^2 and reached 0 mV were classified as APs.

The resting membrane potential was measured immediately after patching the cell and before applying any current. The input resistance was defined as the change in voltage caused by an injection of a hyperpolarizing current, divided by the amount of current. The neuron response to one of the first three negative steps of the alternating currents was used for calculation.

For measuring spike properties, the response elicited by the 200 pA current was used. Spike frequency was measured by dividing the number of action potentials by the current injection time. Spike threshold was defined as the difference between the resting membrane potential and the neuron's membrane potential when spike acceleration went over 20 mV/ms^2 for the first time. Spike amplitude was measured as the difference between the membrane potential at the threshold point and at the peak of the spike. The spike width was defined as the time it took from the spike upstroke's half-maximal amplitude to the same voltage during the repolarizing phase. Finally, spontaneous activity was considered as positive if the patched neuron produced any action potentials within two minutes without any current injection.

Immunocytochemistry

Neuron cultures were fixed for 12 minutes at room temperature by using 3.6 % PFA pH 7.4 with 3 % sucrose. Fixed cultures were blocked with blocking buffer (5 % FBS and 0.1 % Triton X-100 in 1xPBS) for 60 minutes. Then they were probed with primary antibodies overnight at 4 degrees. Secondary antibodies were applied for 1 hr at room temperature. For imaging, Leica DMI4000B microscope (Leica Systems) with Leica TCS SPE confocal system for laser scanning and detection was used. Care was taken to keep the images in linear range. Leica application suite AF software was used for immunofluorescence intensity quantification. In all cases where confocal microscopy was used, image stacks were converted to maximum intensity projection images. All immunofluorescence intensities were calculated by measuring the intensity of the region of interest (ROI), and then subtracting the intensity of a control region adjacent to the ROI to compensate for non-specific staining. Nearby prominent structures were avoided for control regions.

The immunofluorescence intensity of the 0-100 μm region of the axon was considered as the "axon stem signal". For dendrites, the brightest 3 branches were chosen, and the "dendrite

signal" was calculated by averaging the immunofluorescence intensities of the 0-100 μm region of these 3 dendrites. Cell body signal was measured at the soma, by cutting off the dendrite and axon area from their stems. For "400 μm axon signal" and "800 μm axon signal", immunofluorescence intensities of axon regions 350-450 μm and 750-850 μm away from the cell body were measured.

Antibodies

Primary antibodies: VGLUT1 (Synaptic systems, 135-303, RRID:AB_887875), VGAT (Synaptic systems, 131-003, RRID:AB_887869), PSD95 (Thermo Fisher, MA1-04, RRID:AB_325399), Gephyrin (Synaptic systems, 147-011, RRID:AB_887717), extracellular Pan-Neurofascin (NeuroMab, 75-172, RRID:AB_2282826), cleaved caspase 3 (Cell signaling, 9664S, RRID:AB_2070042), Rab11 (Thermo Fisher, 71-5300, RRID:AB_2533987), β3 Tubulin (abcam, ab41489, RRID:AB_727049), SMI312 (abcam, ab24574), Ankyrin G (NeuroMab, 75-146), GFP (Invitrogen, A10262), RFP (abcam, ab62341, RRID:AB_945213), integrin alpha5 (MERCK, AB1928, RRID:AB_2128185).Secondary antibodies: Alexa Fluor 488 goat anti chicken, 568 goat anti rabbit, 660 goat anti mouse (Invitrogen).

Culture of hESC-derived neurons

RC17 clinical grade hESC cells (**RRID:CVCL_L206)** were sourced from Roslin Cells, Scottish Centre for Regenerative Medicine, Edinburgh, United Kingdom. The cell line was genotyped and tested for genetic modifications by Roslin Cells. The cell line is free from mycoplasma contamination as determined by RT-qPCR. Complete details are published (De Sousa et al., 2016) and available online: https://hpscreg.eu/cell-line/RCe021-A

On d0 hESC were detached with EDTA and transferred to form embryoid bodies from d0 to d4 in neural induction medium (Neurobasal:DMEM/F12 (1:1, Gibco, Life Technologies), 0.2%P/S, l-glutamine, N2 (Gibco, Life Technologies), B27 (Thermo Fisher Scientific), supplemented with recombinant Sonic Hedgehog C24II (Shh, 200 μg/ml, R&D systems), recombinant noggin (Ng, 100 μg/ml, R&D systems) SB431542 (SB, 10 mM, R&D systems) and CHIR99021 (CH, 10 mM, Tocris Bioscience). Rock inhibitor (RI, 10 MM, Sigma) was present in the medium from d0 to d2). At d4, embryoid bodies were plated in poly-L-ornithine (0.001%, Sigma-Aldrich), Laminin (4.4 μg/ml, Gibco, Life Technologies) and Fibronectin (PLF) coated plates and cultured in neural proliferation medium (Neurobasal:DMEM/F12 (1:1), 0.5xN2, 0.5xB27, supplemented with Shh, Ng, SB and CH

from d4-d7, and with Shh, Ng and CH from d7-d9). At d11, cells were dissociated with Accutase (Sigma) and $50*10^4$ cells per well single cell suspensions were plated in PLF-coated 8-well chamber slides (Ibidi). Cells were cultured in neuronal differentiation medium (NB with 0.2%P/S, l-glutamine, B27, Ascorbic Acid (200 mM, Sigma), recombinant human Brain-derived Neurotrophic Factor (BDNF, 20µg/ml, R&D systems), Glial-cell line derived Neurotrophic Factor (GDNF, 100µg/ml, R&D systems) which was further supplemented with Dibutyryladenosine 3', 5'-cyclic monophosphate sodium salt (db-CAMP; 50 mM, Sigma) and DAPT (10 mM, TOCRIS) from d14 onwards. Medium was replaced twice weekly up to day 50, after which medium was replaced weekly.

Plasmid transfection

Human neurons were transfected using a modified Lipofectamine 2000 protocol as previously published (van Erp et al., 2015). Per 8-well chamber slide, 1.8ug plasmid DNA was mixed with 3 µl of Lipofectamine 2000 in 200 µl of NB, incubated for 30 min, and then added to the neurons in transfection medium (NB with l-glutamine and B27) at 37°C in 5% CO2 for 45 min. Next, neurons were washed with NB, the original conditioned medium was replaced, and cells were cultured for 2 days at 37°C in 5% CO2.

Laser-mediated axotomy of hESC-derived neurons

Selection of neurons and conditions of axotomy were as described for rodent neurons. An Andor spinning disk confocal microscope with temperature and CO2 controlled live imaging chamber was used. GFP-transfected neurons were selected and the axon was identified based on morphology. For axotomy, a MicroPoint photo-stimulation tool with 365nm laser in combination with a 40xH2O objective were used. The distance from the cell body was kept similar for all experiments (between 300-500um). Both axon and cell body were imaged for 16hours following axotomy with 20min intervals using a 20x objective and minimal laser intensity to reduce the risk of phototoxicity. Neuronal survival was high (typically 100%). Axotomy results were manually analysed using Fiji.

Immunocytochemistry:

For human neurons, cells were fixed by addition of 8%PFA to equal volume of culture medium (final concentration 4%) and incubating for 15min at RT. Then cultures were blocked for 30min at RT in blocking buffer (2% Normal Horse Serum, 2% Normal Goat Serum, 1% bovine serum albumin (BSA), 0.2% Triton X-100) followed by overnight incubation with primary antibodies in blocking buffer. The following day, samples were incubated with secondary antibodies diluted in blocking buffer for 60min at RT. Images were

taken using a Leica TCS SP8 confocal microscope with 40x objective. Axons were identified using *SMI312 (Biolegend).*

Quantification of integrin alpha5 axon-dendrite ratio

Cortical neurons were transfected at DIV10 with either GFP or Rab11WT and fixed at DIV14 with methanol. These were immunolabelled for integrin alpha5 and GFP. Control and rab11 transfected cultures were fixed and labelled together, using identical conditions. Images were acquired by confocal laser scanning microscopy using a Leica TCS SPE confocal microscope, using identical settings for each image. Images were acquired at 40x to include the cell body, dendrites and the proximal section of axon in each image. Leica LAS AF software was used to measure mean fluorescnece in the axon, and in two dendrites (to give a mean dendrite measurement). A region next to each neurite was used to subtract background fluorescence. Axon dendrite-ratio was determined as the mean dendrite fluorescence intensity divided by the axon intensity. GraphPad Prism (RRID:SCR_002798) was used for statistical analysis of data using a students T-Test.

Statistics

Statistics were performed using GraphPad Prism and the program R. Kolmogorov–Smirnov test was used for normality testing. For comparison of 2 sample groups, t-test was used. Student's or Welch's t-test was used depending on the variance. For comparison of more than 2 groups, one-way ANOVA was normally used. For the post hoc test, Bonferroni's, or Dunnett's post hoc test was used depending on the comparisons that were going to be made. For the cases where the assumption of equal variance was significantly violated (determined by Bartlett's test), Games-Howell post hoc test was used. Some of the patch clamp results and many of the axotomy results violated the normal distribution assumption. For the patch clamp results, Kruskal-Wallis test was used instead of one-way ANOVA. For the axotomy results, the data was converted by log10 to shift it to normal distribution. For regeneration ratio results, fisher's exact test was used, and Bonferroni correction was applied for repeated comparisons. For the Rab11 vesicle movement analysis, two-way ANOVA was used, followed by a Bonferroni's post hoc test.

Acknowledgments

The work was supported by grants from the Glaxo Smith Kline International Scholarship (to H.K.), Honjo International Scholarship (to H.K.), Bristol-Myers Squibb Graduate Studentship (to H.K.), the Christopher and Dana Reeve Foundation, the Medical Research Council, the ERC advanced grant ECMneuro, the NIHR Cambridge Biomedical Research Centre and the Operational Programme Research, Development and Education in the framework of the project "Centre of Reconstructive Neuroscience", registration number CZ.02.1.01/0.0./0.0/15_003/0000419

References

Andrews, M.R., Czvitkovich, S., Dassie, E., Vogelaar, C.F., Faissner, A., Blits, B., Gage, F.H., ffrench-Constant, C., and Fawcett, J.W. (2009). Alpha9 integrin promotes neurite outgrowth on tenascin-C and enhances sensory axon regeneration. J. Neurosci. 29, 5546–57.

Andrews, M.R., Soleman, S., Cheah, M., Tumbarello, D.A., Mason, M.R.J., Moloney, E., Verhaagen, J., Bensadoun, J.-C., Schneider, B., Aebischer, P., et al. (2016). Axonal Localization of Integrins in the CNS Is Neuronal Type and Age Dependent. eNeuro 3, ENEURO.0029–16.2016.

Ascaño, M., Richmond, A., Borden, P., and Kuruvilla, R. (2009). Axonal targeting of Trk receptors via transcytosis regulates sensitivity to neurotrophin responses. J. Neurosci. 29, 11674–85.

Baetz, N.W., and J.R. Goldenring. 2013. Rab11-family interacting proteins define spatially and temporally distinct regions within the dynamic Rab11a-dependent recycling system. *Mol. Biol. Cell*. 24:643-658.

Barbati, A.C., C. Fang, G.A. Banker, and B.J. Kirby. 2013. Culture of primary rat hippocampal neurons: design, analysis, and optimization of a microfluidic device for cell seeding, coherent growth, and solute delivery. *Biomed. Microdevices*. 15:97-108.

Bareyre, F.M., M. Kerschensteiner, O. Raineteau, T.C. Mettenleiter, O. Weinmann, and M.E. Schwab. 2004. The injured spinal cord spontaneously forms a new intraspinal circuit in adult rats. *Nat. Neurosci*. 7:269-277.

Bentley, M., and Banker, G. (2016). The cellular mechanisms that maintain neuronal polarity. Nat. Rev. Neurosci. 17, 611–22.

Bernstein-Goral, H., and B.S. Bregman. 1993. Spinal cord transplants support the regeneration of axotomized neurons after spinal cord lesions at birth: A quantitative double-labeling study. *Exp. Neurol*. 123:118-132.

Britt, D.J., G.G. Farias, C.M. Guardia, and J.S. Bonifacino. 2016. Mechanisms of Polarized Organelle Distribution in Neurons. *Front Cell Neurosci*. 10:88.

van Bergeijk, P., Adrian, M., Hoogenraad, C.C., and Kapitein, L.C. (2015). Optogenetic control of organelle transport and positioning. Nature 518, 111–114.

Bradke, F., Fawcett, J.W., and Spira, M.E. (2012). Assembly of a new growth cone after axotomy: the precursor to axon regeneration. Nat. Rev. Neurosci. 13, 183–93.

Britt, D.J., Farías, G.G., Guardia, C.M., and Bonifacino, J.S. (2016). Mechanisms of Polarized Organelle Distribution in Neurons. Front. Cell. Neurosci. 10, 88.

Byrne, A.B., Walradt, T., Gardner, K.E., Hubbert, A., Reinke, V., and Hammarlund, M. (2014). Insulin/IGF1 Signaling Inhibits Age-Dependent Axon Regeneration. Neuron 81, 561–573.

Canty, A.J., Teles-Grilo Ruivo, L.M., Nesarajah, C., Song, S., Jackson, J.S., Little, G.E., and De Paola, V. (2013). Synaptic elimination and protection after minimal injury depend on cell type and their prelesion structural dynamics in the adult cerebral cortex. J. Neurosci. 33, 10374–83.

Caswell, P.T., and J.C. Norman. 2006. Integrin trafficking and the control of cell migration. *Traffic*. 7:14-21.

Cheah, M., Andrews, M.R., Chew, D.J., Moloney, E.B., Verhaagen, J., Fässler, R., and Fawcett, J.W. (2016). Expression of an Activated Integrin Promotes Long-Distance Sensory Axon Regeneration in the Spinal Cord. J. Neurosci. 36, 7283–97.

De Sousa, P.A., Tye, B.J., Bruce, K., Dand, P., Russell, G., Collins, D.M., Greenshields, A., McDonald, K., Bradburn, H., Allan, D., et al. (2016). Derivation of the clinical grade human embryonic stem cell line RCe021-A (RC-17). Stem Cell Res 17, 1-5.

Du, K., Zheng, S., Zhang, Q., Li, S., Gao, X., Wang, J., Jiang, L., and Liu, K. (2015). Pten Deletion Promotes Regrowth of Corticospinal Tract Axons 1 Year after Spinal Cord Injury. J. Neurosci. 35, 9754–63.

Eva, R., Crisp, S., Marland, J.R.K., Norman, J.C., Kanamarlapudi, V., ffrench-Constant, C., and Fawcett, J.W. (2012). ARF6 directs axon transport and traffic of integrins and regulates axon growth in adult DRG neurons. J. Neurosci. 32, 10352–64.

Eva, R., Dassie, E., Caswell, P.T., Dick, G., ffrench-Constant, C., Norman, J.C., and Fawcett, J.W. (2010). Rab11 and its effector Rab coupling protein contribute to the trafficking of beta 1 integrins during axon growth in adult dorsal root ganglion neurons and PC12 cells. J. Neurosci. 30, 11654–69.

Fawcett, J.W., Schwab, M.E., Montani, L., Brazda, N., and Müller, H.W. (2012). Defeating inhibition of regeneration by scar and myelin components. Handb. Clin. Neurol. 109, 503–22.

Franssen, E.H.P., Zhao, R.-R., Koseki, H., Kanamarlapudi, V., Hoogenraad, C.C., Eva, R., and Fawcett, J.W. (2015). Exclusion of integrins from CNS axons is regulated by Arf6 activation and the AIS. J. Neurosci. 35, 8359–75.

Geoffroy, C.G., Hilton, B.J., Tetzlaff, W., Zheng, B., Anderson, M.A., Ao, Y., Sofroniew, M.V., Badan, I., Buchhold, B., Hamm, A., et al. (2016). Evidence for an Age-Dependent Decline in Axon Regeneration in the Adult Mammalian Central Nervous System. Cell Rep. 15, 238–246.

Harris, W.A., C.E. Holt, and F. Bonhoeffer. 1987. Retinal axons with and without their somata, growing to and arborizing in the tectum of xenopus embryos: a time-lapse video study of single fibres in vivo. *Development*. 101:123-133.

Hollis, E.R., Jamshidi, P., Löw, K., Blesch, A., Tuszynski, M.H., and Tuszynski, M.H. (2009). Induction of corticospinal regeneration by lentiviral trkB-induced Erk activation. Proc. Natl. Acad. Sci. U. S. A. 106, 7215–20.

Hollis, E.R., P. Lu, A. Blesch, and M.H. Tuszynski. 2009b. IGF-I gene delivery promotes corticospinal neuronal survival but not regeneration after adult CNS injury. *Exp. Neurol*. 215:53-59.

Hulsbusch, N., G.P. Solis, V.L. Katanaev, and C.A. Stuermer. 2015. Reggie-1/Flotillin-2 regulates integrin trafficking and focal adhesion turnover via Rab11a. *Eur J Cell Biol*. 94:531-545.

Hur, E.M., Saijilafu, and F.Q. Zhou. 2012. Growing the growth cone: remodeling the cytoskeleton to promote axon regeneration. *Trends Neurosci*. 35:164-174.

Kadoya, K., P. Lu, K. Nguyen, C. Lee-Kubli, H. Kumamaru, L. Yao, J. Knackert, G. Poplawski, J.N. Dulin, H. Strobl, Y. Takashima, J. Biane, J. Conner, S.C. Zhang, and M.H. Tuszynski. 2016. Spinal cord reconstitution with homologous neural grafts enables robust corticospinal regeneration. *Nat Med*. 22:479-487.

Jakeman, L.B., and Reier, P.J. (1991). Axonal projections between fetal spinal cord transplants and the adult rat spinal cord: a neuroanatomical tracing study of local interactions. J. Comp. Neurol. 307, 311–34.

Kaech, S., and Banker, G. (2006). Culturing hippocampal neurons. Nat. Protoc. 1, 2406–15.

Kay, L., Humphreys, L., Eickholt, B.J., and Burrone, J. (2011). Neuronal activity drives matching of pre- and postsynaptic function during synapse maturation. Nat. Neurosci. 14, 688–690.

Kim, B.G., Dai, H.-N., Lynskey, J. V, McAtee, M., and Bregman, B.S. (2006). Degradation of chondroitin sulfate proteoglycans potentiates transplant-mediated axonal remodeling and functional recovery after spinal cord injury in adult rats. J. Comp. Neurol. 497, 182–98.

Kirkeby, A., S. Grealish, D.A. Wolf, J. Nelander, J. Wood, M. Lundblad, O. Lindvall, and M. Parmar. 2012. Generation of regionally specified neural progenitors and functional neurons from human embryonic stem cells under defined conditions. *Cell Rep*. 1:703-714.

Lasiecka, Z.M., and Winckler, B. (2011). Mechanisms of polarized membrane trafficking in neurons -- focusing in on endosomes. Mol. Cell. Neurosci. 48, 278–87.

Liu, K., Lu, Y., Lee, J.K., Samara, R., Willenberg, R., Sears-Kraxberger, I., Tedeschi, A., Park, K.K., Jin, D., Cai, B., et al. (2010). PTEN deletion enhances the regenerative ability of adult corticospinal neurons. Nat. Neurosci. 13, 1075–1081.

Liu, K., Tedeschi, A., Park, K.K., and He, Z. (2011). Neuronal intrinsic mechanisms of axon regeneration. Annu. Rev. Neurosci. 34, 131–52.

Lu, P., Y. Wang, L. Graham, K. McHale, M. Gao, D. Wu, J. Brock, A. Blesch, E.S. Rosenzweig, L.A. Havton, B. Zheng, J.M. Conner, M. Marsala, and M.H. Tuszynski. 2012. Long-distance growth and connectivity of neural stem cells after severe spinal cord injury. *Cell*. 150:1264-1273.

Macia, E., M. Partisani, C. Favard, E. Mortier, P. Zimmermann, M.F. Carlier, P. Gounon, F. Luton, and M. Franco. 2008. The pleckstrin homology domain of the Arf6-specific exchange factor EFA6 localizes to the plasma membrane by interacting with phosphatidylinositol 4,5-bisphosphate and F-actin. *J. Biol. Chem*. 283:19836-19844.

Maeder, C.I., Shen, K., and Hoogenraad, C.C. (2014). Axon and dendritic trafficking. Curr. Opin. Neurobiol. 27, 165–70.

Matsuzaki, F., M. Shirane, M. Matsumoto, and K.I. Nakayama. 2011. Protrudin serves as an adaptor molecule that connects KIF5 and its cargoes in vesicular transport during process formation. *Mol. Biol. Cell*. 22:4602-4620.

Montagnac, G., J.B. Sibarita, S. Loubery, L. Daviet, M. Romao, G. Raposo, and P. Chavrier. 2009. ARF6 Interacts with JIP4 to control a motor switch mechanism regulating endosome traffic in cytokinesis. *Curr. Biol*. 19:184-195.

Park, M., Salgado, J.M., Ostroff, L., Helton, T.D., Robinson, C.G., Harris, K.M., and Ehlers, M.D. (2006). Plasticity-induced growth of dendritic spines by exocytic trafficking from recycling endosomes. Neuron 52, 817–30.

Petersen, J.D., S. Kaech, and G. Banker. 2014. Selective microtubule-based transport of dendritic membrane proteins arises in concert with axon specification. *J Neurosci*. 34:4135-4147.

Ramel, D., Wang, X., Laflamme, C., Montell, D.J., and Emery, G. (2013). Rab11 regulates cell-cell communication during collective cell movements. Nat. Cell Biol. 15, 317–24.

Sheehan, D., Ray, G.S., Calhoun, B.C., and Goldenring, J.R. (1996). A somatodendritic distribution of Rab11 in rabbit brain neurons. Neuroreport 7, 1297–300.

Randazzo, P.A., K. Miura, Z. Nie, A. Orr, A.B. Theibert, and B.G. Kearns. 2001. Cytohesins and centaurins: mediators of PI 3-kinase regulated Arf signaling. *Trends Biochem Sci*. 26:220-221.

Reier, P.J., B.S. Bregman, and J.R. Wujek. 1986. Intraspinal transplantation of embryonic spinal cord tissue in neonatal and adult rats. *J. Comp Neurol*. 247:275-296.

Richardson, P.M., V.M.K. Issa, and A.J. Aguayo. 1984. Regeneration of long spinal axons in the rat. *J. Neurocytol*. 13:165-182.

Rosenzweig, E.S., G. Courtine, D.L. Jindrich, J.H. Brock, A.R. Ferguson, S.C. Strand, Y.S. Nout, R.R. Roy, D.M. Miller, M.S. Beattie, L.A. Havton, J.C. Bresnahan, V.R. Edgerton, and M.H. Tuszynski. 2010. Extensive spontaneous plasticity of corticospinal projections after primate spinal cord injury. *Nat. Neurosci*. 13:1505-1510.

Tosney, K.W., and L.T. Landmesser. 1985. Growth cone morphology and trajectory in the lumbosacral region of the chick embryo. *J. Neurosci*. 5:2345-2358.

Shirane, M., and Nakayama, K.I. (2006). Protrudin induces neurite formation by directional membrane trafficking. Science 314, 818–21.

Tan, C.L., Kwok, J.C.F., Patani, R., Ffrench-Constant, C., Chandran, S., and Fawcett, J.W. (2011). Integrin activation promotes axon growth on inhibitory chondroitin sulfate proteoglycans by enhancing integrin signaling. J. Neurosci. 31, 6289–95.

Tang, N.H., and Chisholm, A.D. (2016). Regulation of Microtubule Dynamics in Axon Regeneration: Insights from C. elegans. F1000Research 5.

van Erp, S., D.M. van den Heuvel, Y. Fujita, R.A. Robinson, A.J. Hellemons, Y. Adolfs, E.Y. Van Battum, A.M. Blokhuis, M. Kuijpers, J.A. Demmers, H. Hedman, C.C. Hoogenraad, C. Siebold, T. Yamashita, and R.J. Pasterkamp. 2015. Lrig2 Negatively Regulates Ectodomain Shedding of Axon Guidance Receptors by ADAM Proteases. *Dev Cell*. 35:537-552.

Welz, T., Wellbourne-Wood, J., Kerkhoff, E., Salminen, A., Novick, P.J., Bos, J.L., al., et, D'Souza-Schorey, C., Chavrier, P., Stenmark, H., et al. (2014). Orchestration of cell surface proteins by Rab11. Trends Cell Biol. 24, 407–15.

Figure Legends

Figure 1

Electrical and anatomical maturation of neurons.

(A) Resting membrane potential of maturing neurons. The average membrane potential from at least 3 patching sessions is shown. At least 10 neurons per session. One-way ANOVA followed by Bonferroni's post hoc test.

(B) Membrane capacitance of maturing neurons. One-way ANOVA followed by Games-Howell post hoc test.

(C) Percentage of patched neurons capable of firing action potentials when depolarizing currents were applied. The average percentage from at least 3 patching sessions is shown. At least 10 neurons/session. At 24 DIV, all neurons fired action potentials. Representative responses are shown in (E).

(D) Percentage of neurons showing spontaneous activity. Fisher's exact test.

Error bars represent s.e.m. Patch clamp results from at least 3 independent sessions were accumulated. Sample numbers are shown in the figure.

* $p < 0.05$, ** $p < 0.01$, *** $p < 0.001$ and **** $p < 0.0001$.

Further details are in Figure1 Figure Supplement 1

(A,B,C) Quantification of spike properties plotted by DIV. Spike amplitude (A), width (B), and frequency (C) were measured. A: One-way ANOVA followed by Bonferroni's post hoc test. B,C: Kruskal-Wallis test.

(D,E) Spike threshold and input resistance of maturing neurons. D: One-way ANOVA followed by Games-Howell post hoc test. E: Kruskal-Wallis test.

(F) Excitatory and inhibitory synapse formation at 10 DIV and 20 DIV. Excitatory synapses were marked with VGLUT1 and PSD95, and inhibitory synapses were marked with VGAT and gephyrin.

(K) Percentage of neurons showing spontaneous activity. Fisher's exact test.

Error bars represent s.e.m.. * $p < 0.05$, ** $p < 0.01$, *** $p < 0.001$ and **** $p < 0.0001$.

Figure 1 Figure supplement 2

A) staining of cultures at 3,7 and 14 days for two maturity markers, doublecortin and low molecular weight neurofilament. B),C) plots of the intensity of immunofluorescence and the mRNA levels of the two maturity markers. F) mRNA levels of Rab11a and Rab11b from the mRNA profile. D) Two categories of molecules that showed large expression changes in the mRNA profiling from ingenuity analysis.

Figure 1 Figure supplement 3

A) Live neurofascin staining at 4 and 16 DIV to show staining of the axon initial segment. B) caspase 3 staining of a GFP transfected 24 DIV culture, showing no signs of apoptosis and staining of a staurosporine treated culture as a positive control.

Figure 2

(A,B) Representative images of death, branch loss, bulb formation. Axotomy location is indicated by the yellow star.

(G) Ratio of bulb formation, branch loss and cell death categorized by DIV. Fisher's exact test with Bonferroni correction.

Figure 3

Regeneration after axotomy.

(A) An axon before cutting, followed by retraction bulb formation and regeneration.

(B) A further example of regeneration after axotomy and an example of ectopic growth.

(C) The overall proportion of axons showing the different forms of behaviour after axotomy at different stages of maturity.

Figure 4

Maturation related changes in retraction and regeneration.

(A) Relative frequency plot of retraction distance categorized by DIV. Average distance comparison between 4 DIV and 24 DIV: Welch's t-test.

(B) Retraction distance categorized separately by DIV, retraction, and axotomy distance. 16 DIV: One-way ANOVA followed by Bonferroni's post hoc test, 24 DIV: Welch's t-test.

(C) Regeneration ratio categorized by DIV, retraction, and axotomy distance. 16 DIV: Fisher's exact test with Bonferroni correction, 16 DIV proximal axotomy vs 24 DIV proximal axotomy: Fisher's exact test, 24 DIV: Fisher's exact test.

(D,E,F) Regeneration initiation time, regeneration length and growth cone area categorized by DIV. One-way ANOVA followed by Games-Howell post hoc test.

(G) Plot of regeneration success against log retraction distance.

Error bars represent s.e.m.. Axotomy results were accumulated from at least 3 independent axotomy sessions. Retraction distance was converted by log10. * $p < 0.05$, ** $p < 0.01$, *** $p < 0.001$ and **** $p<0.0001$.

Further analyses are in **Figure 4 Figure Supplement 1.**

(A and B) Retraction distance and retraction bulb formation time categorized by DIV. Kruskal-Wallis test.

(C) Correlation between retraction distance and retraction bulb formation time.

(D and E) Retraction distance plotted against axotomy distance. Retraction distance was categorized by DIV and retraction group.

(F,G,H) Regeneration initiation time (F), regeneration length (G), and growth cone area (H) of regenerating 16 DIV neurons categorized by retraction and axotomy distance. Categorization by retraction distance groups did not lead to any obvious trends. One-way ANOVA followed by Bonferroni's post hoc test. Regeneration length showed a declining trend with axotomy distance ($p=0.0618$, Student's t-test).

Error bars represent s.e.m.. Axotomy results were accumulated from at least 3 independent sessions. Sample numbers are described in the figure.

* $p < 0.05$, ** $p < 0.01$, *** $p < 0.001$ and **** $p<0.0001$.

Figure 5

Decline in regeneration is not due to the mature environment.

(A) GFP transfected E18 cortical neurons were plated on either PDL glass or 21 DIV cultures, and cultured for 4 days.

(B and C) Quantification of axon length (B) and branch numbers (C) 4 days after plating on PDL or 21 DIV cultures. n=3 independent cultures, at least 20 neurons/culture. Student's t-test.

(D) Relative frequency plot of retraction distance categorized by DIV and plating surface. Distal axotomy results were compared. 4 DIV on 25 DIV vs 24 DIV on PDL: Student's t-test.

(E) Regeneration ratio categorized by DIV and plating surface. Distal axotomy results were compared. Fisher's exact test.

One-way ANOVA followed by Games-Howell post hoc test. Error bars represent s.e.m. Retraction distance was converted by log10. * $p < 0.05$, ** $p < 0.01$ and **** $p < 0.0001$.

Figure 6

Endogenous Rab11 becomes restricted to the somatodenritic domain with maturation

(A) Immunofluorescence staining of Rab11 in 4 and 24 DIV neurons. Neurons were co-stained with beta-3 tubulin or GFP for neuronal outline, and SMI312 or Ankyrin-G for axon marking.

(B, C and D) Quantification of Rab11 immunofluorescence intensity. Immunofluorescence intensities of the cell body, axon stem and proximal dendrite were measured, and ratios were calculated. Staining conditions were kept consistent and images were acquired under the same exposure. n=3 independent cultures.

Figure 7

(A and B) Axon stem/proximal dendrite ratio (A) and axon stem signal intensity (B) of total Rab11 (both transfected and endogenous) in cytosolic GFP or Rab11a WT overexpressed neurons. Transfected neurons were immunofluorescently labelled with Rab11 antibody and quantified. n=3 independent staining, Welch's t-test.

(C) Axon stem/proximal dendrite immunofluorescence intensity ratio of transfected neurons. Neurons were transfected with cytosolic GFP or fluorescence-tagged Rab11a forms, and the fluorescent protein was probed by immunofluorescence staining.

(D) Comparison of fluorescence signal between proximal and distal axon. Distal axon intensity was divided by axon stem intensity.

(E) Representative kymographs of fluorescence-tagged Rab11a forms in axon stems and proximal dendrites.

(F) Quantification of vesicular movements in neurons overexpressing fluorescence-tagged Rab11a forms. Images were acquired every second for 3 minutes, and kymographs were produced from a 30 μm region of the axon stem or proximal dendrite. Vesicle movement direction (F) and average vesicle velocity (retrograde and anterograde Fig. S5A,B) were quantified.

Error bars represent s.e.m.. Rab11 overexpression results of E~K were accumulated from at least 3 independent transfected cultures. Sample numbers are described in the figure. (B~G) One-way ANOVA followed by Bonferroni's post hoc test. (I~K) Two-way ANOVA followed by Bonferroni's post hoc test. Black asterisks: axon and dendrite comparison, blue asterisks: Rab11 type comparison. * $p < 0.05$, ** $p < 0.01$, *** $p < 0.001$ and **** $p < 0.0001$.

Further details are in **Figure 7 Figure supplement 1**

(A,B) Quantification of vesicular movements in neurons overexpressing fluorescence-tagged Rab11a forms. Images were acquired every second for 3 minutes, and kymographs were produced from a 30 μm region of the axon stem or proximal dendrite. Average vesicle velocity was quantified.

Error bars represent s.e.m.. Sample numbers are described in the figure. Two-way ANOVA followed by Bonferroni's post hoc test. Black asterisks: axon and dendrite comparison, blue asterisks: Rab11 type comparison. * $p < 0.05$, ** $p < 0.01$, *** $p < 0.001$ and **** $p < 0.0001$.

Figure 8

Rab11a overexpression increases intra-axonal Rab11 and enhances regeneration.

(A) Accumulation of overexpressed Rab11a WT at the retraction bulb. Note how Rab11a accumulation can start earlier than GFP.

(B,C) Retraction distance and retraction bulb formation time correlate (B), and the frequency plot of retraction distance takes a biphasic distribution (C) in Rab11a transfected neurons.

(D,E,F) Retraction distance (F and G) and regeneration ratio (H) of Rab11a overexpressed neurons categorized by retraction group and form. F, G: One-way ANOVA followed by Dunnett's post hoc test. H: Fisher's exact test with Bonferroni correction.

(G,H,I) Regeneration initiation time, regeneration length and growth cone area of Rab11a overexpressed neurons categorized by Rab11 type. One-way ANOVA followed by Dunnett's post hoc test.

Error bars represent s.e.m.. Axotomy results were accumulated from at least 3 independent sessions. Retraction distance was converted by log10. Sample numbers are described in the figure. * $p < 0.05$, ** $p < 0.01$ and *** $p < 0.001$.

Figure 9

Rab11 forced into axons by overexpression carries α5 integrin with it. DIV 10 neurons were transfected with either Rab11-GFP or control GFP, then fixed and immunolabelled on DIV16. A) left shows that in control cells GFP enters dendrites and the axon identified by neurofascin staining, while α5 integrin is excluded. On the right, Rab11-GFP is transfected, and mistrafficks into the proximal axon. The axon now contains plentiful α5 integrin. The distribution of α5 integrin between axons and dendrites is quantified in B) and C) as fluorescence intensity levels and axon/dendrite intensity ratio. Bar=25μm, ***= P<001by T test.

Figure 10

Age-dependent decline in axonal regeneration of hESC-derived neurons is partially rescued by increasing intra-axonal Rab11 levels.

A. hESC-derived neurons show an age-related decrease in regeneration following laser-mediated axotomy. Overexpression of Rab11-WT improves the percentage of regenerated axons in d45-55 neurons. n=4 independent experiments per time point. **B-C.** Axonal levels of Rab11-GFP decline in mature hESC-derived neurons as compared to dendritic levels. Axons were identified using SMI-312 immunolabeling and intensity of GFP immunolabeling was measured. n>3 independent stainings. **D.** Regeneration length measured at 2hrs after initiation of regeneration is increased in Rab11 overexpressing hESC-derived neurons. n=16 for both for GFP and Rab11+GFP, collected from four independent experiments. **E.** Retraction distance distribution is not affected by Rab11 overexpression in hESC-derived neurons. n=22 and 23 for GFP and Rab11+GFP respectively, collected from four

independent experiments. In all graphs, error bars represent S.E.M. *p<0.05. Unpaired t-test, Welch's correction.

Videos

Video 1 shows successful regeneration of an axon from an immature neuron, cut at 4 DIV.

Video 2 shows failure of regeneration of an axon from a mature neuron, cut at 30 DIV.

Video 3 shows an example of a neuron transfected with Rab11 DN-RFP and GFP, showing that Rab11 appears in the stump soon after axotomy and is present in the growth cone throughout regeneration and growth.

Table

Table 1 shows the terms used in the paper to describe regeneration and their definition

1038

Author Contributions

H.K. designed the project, performed experiments, interpreted data, and wrote the manuscript. M.D. performed electrophysiology experiments and analyzed the data. B.Y.H.L and G.S.H.Y supervised the RNA sequencing and data analysis. V.P. performed experiments. S.vE. performed experiments, interpreted data, and provided material. J.C.F.K. oversaw experimental design. C. ff-C. designed the project, and interpreted data. R.E. designed the project, performed experiments, interpreted data, and provided material. J.W.F designed and supervised the project, interpreted data, and wrote the manuscript.

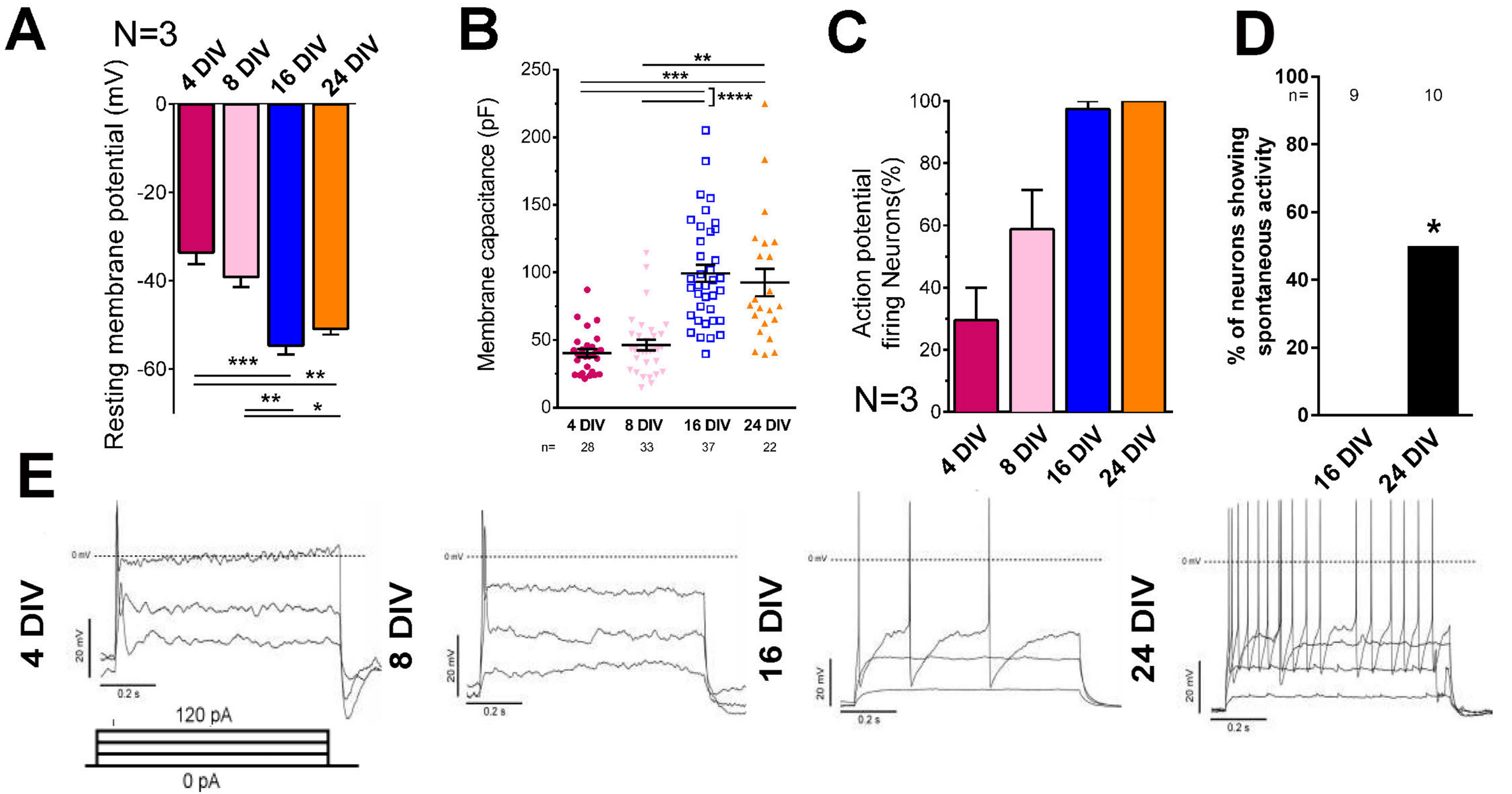
A
N=3
4 DIV
8 DIV
16 DIV
24 DIV
Resting membrane potential (mV)
0
-20
-40
-60
***
**
**
*
B
Membrane capacitance (pF)
250
200
150
100
50
0
**
***
****
4 DIV
8 DIV
16 DIV
24 DIV
n=
28
33
37
22
C
Action potential firing Neurons(%)
100
80
60
40
20
0
N=3
4 DIV
8 DIV
16 DIV
24 DIV
D
% of neurons showing spontaneous activity
100
80
60
40
20
0
n=
9
10
*
16 DIV
24 DIV
E
4 DIV
8 DIV
16 DIV
24 DIV
0 mV
20 mV
0.2 s
120 pA
0 pA

Figure 1

Spike properties

Exitability

Network development

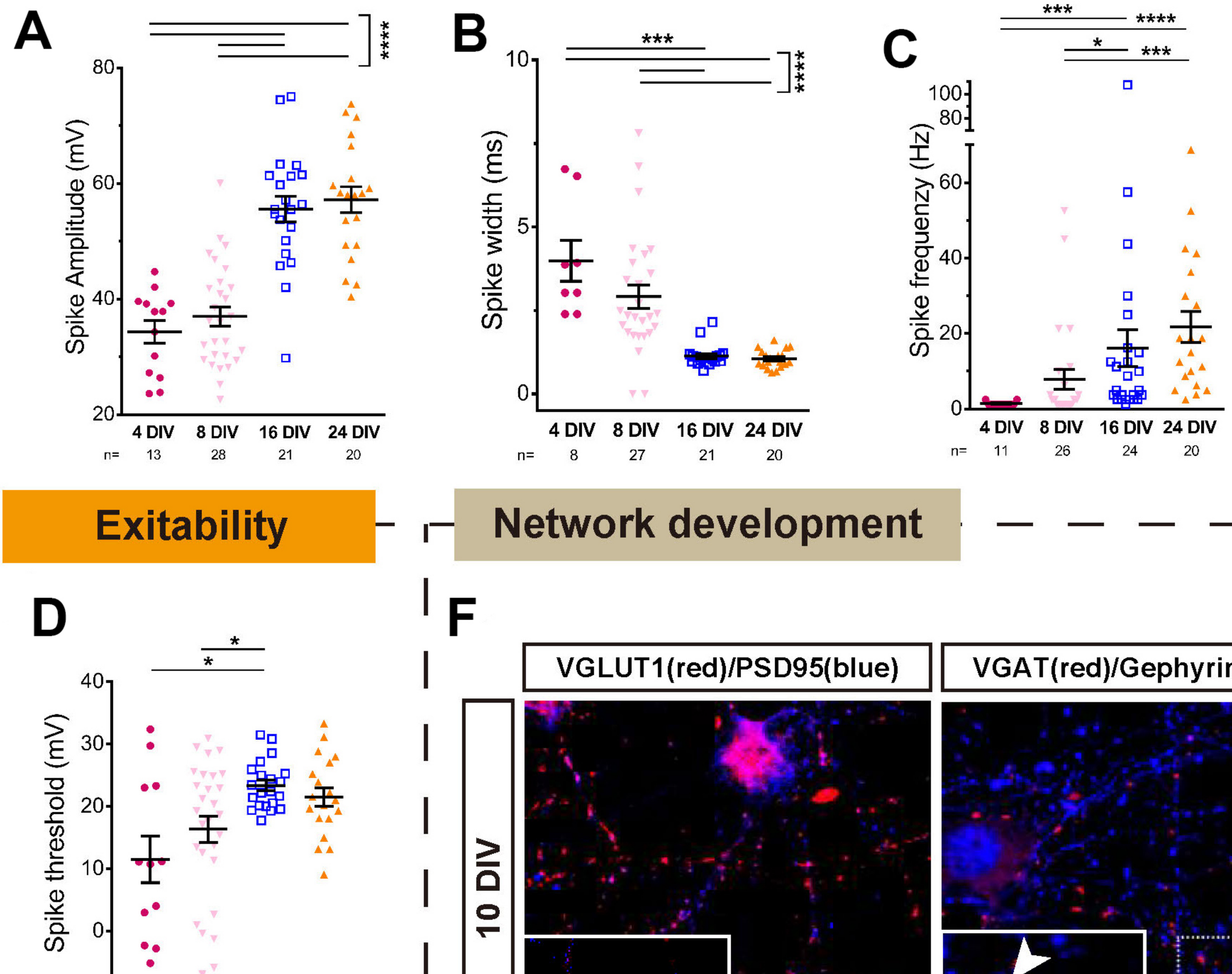

Figure 1 supplementary figure 1

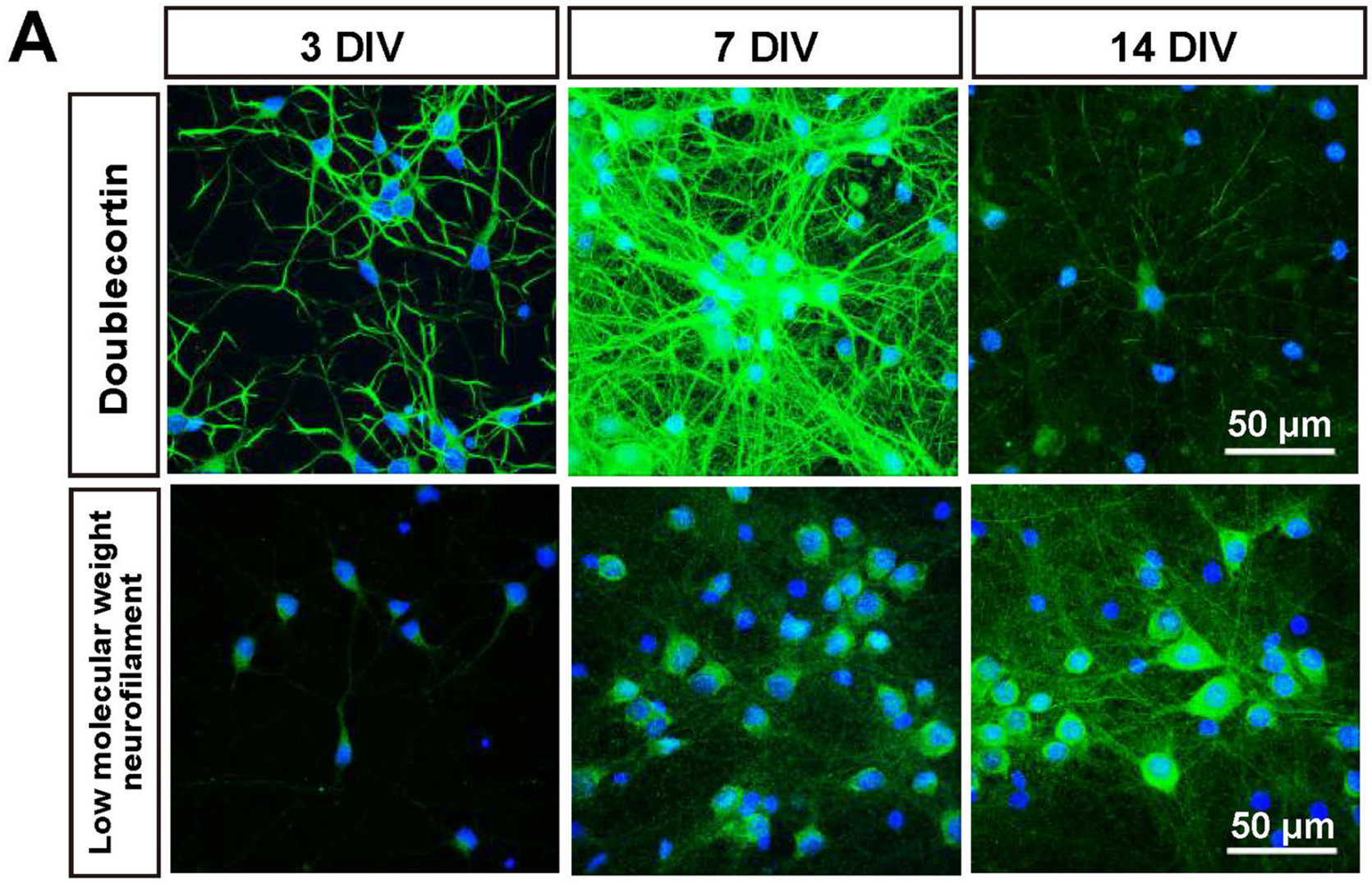

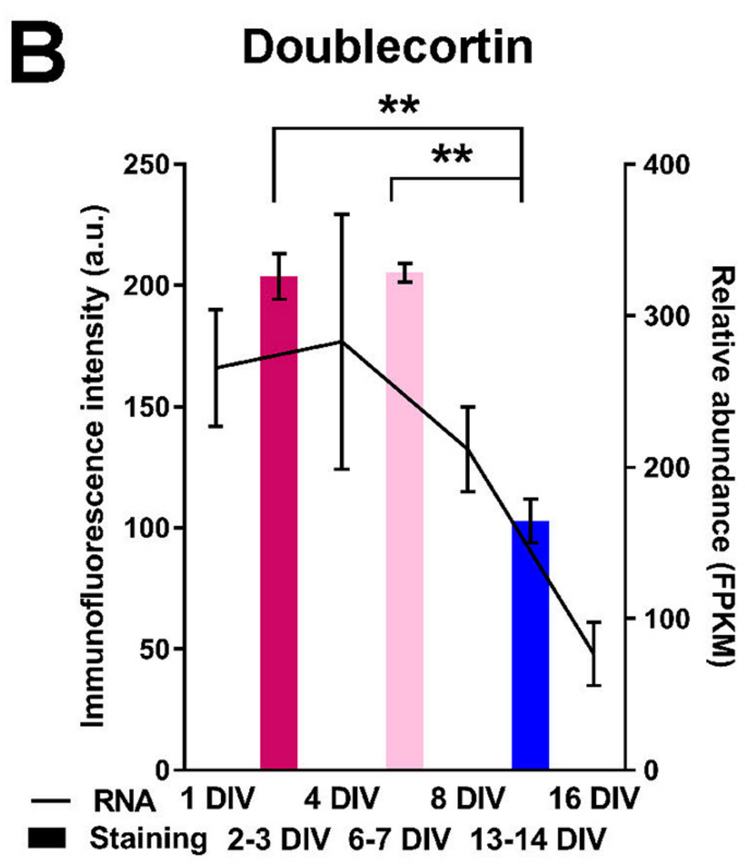

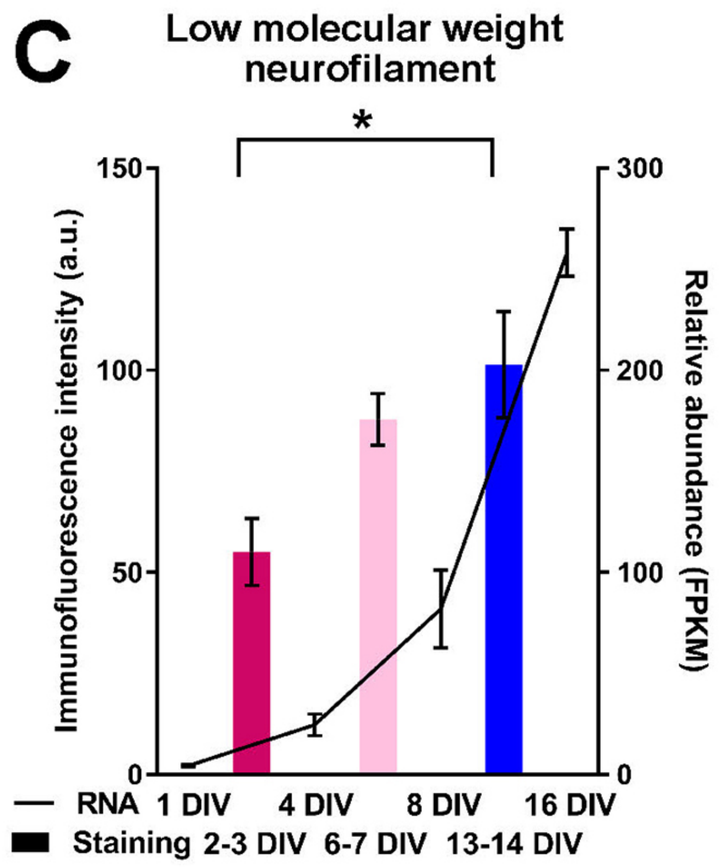

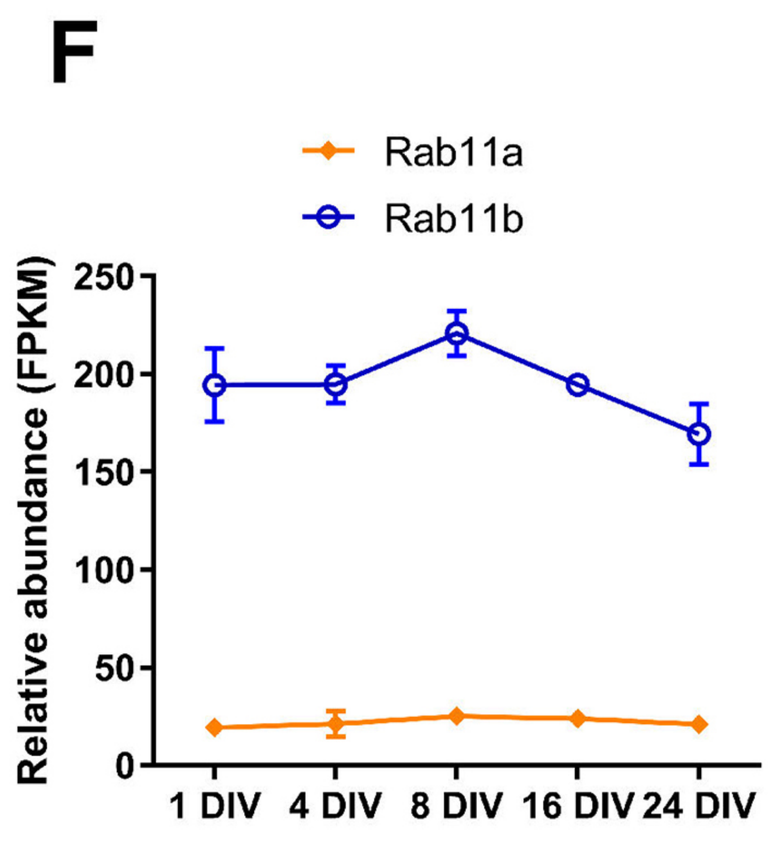

D

Top 5 functional analysis of genes increasing expression with DIV

Categories	Functions	p-Value
Cell-To-Cell Signaling and Interaction, Nervous System Development and Function	neurotransmission	3.84E-52
Cell-To-Cell Signaling and Interaction, Nervous System Development and Function	synaptic transmission	2.80E-46
Cell-To-Cell Signaling and Interaction, Nervous System Development and Function	long-term potentiation	6.12E-31
Molecular Transport	transport of molecule	1.64E-26
Cell-To-Cell Signaling and Interaction, Nervous System Development and Function	excitatory postsynaptic potential	1.94E-25

E

Top 5 functional analysis of genes decreasing expression with DIV

Categories	Functions	p-Value
Gene Expression	transcription of DNA	3.68E-25
Organismal Survival	organismal death	5.96E-19
Cellular Growth and Proliferation	proliferation of cells	3.60E-18
Nervous System Development and Function	development of central nervous system	3.95E-18
Embryonic Development, Organismal Development	development of body axis	9.56E-17

Figure 1 supplementary figure 2

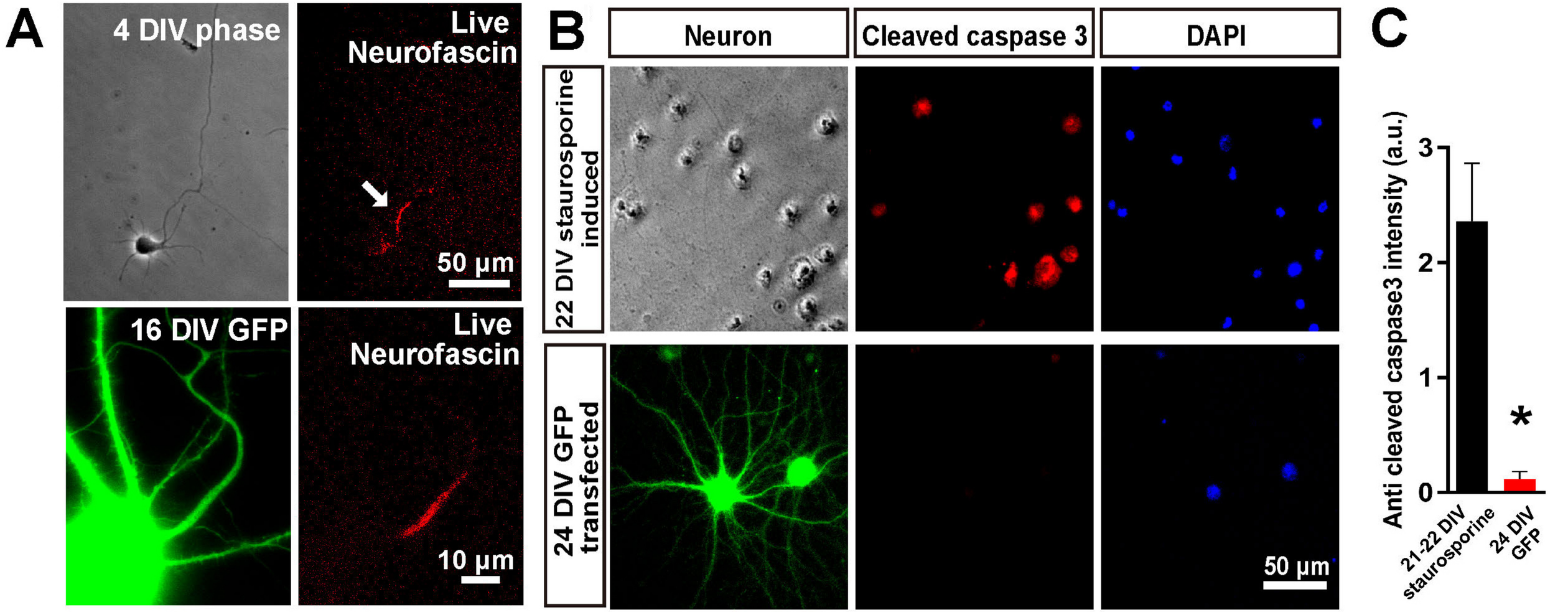

Figure 1 supplementary figure 3

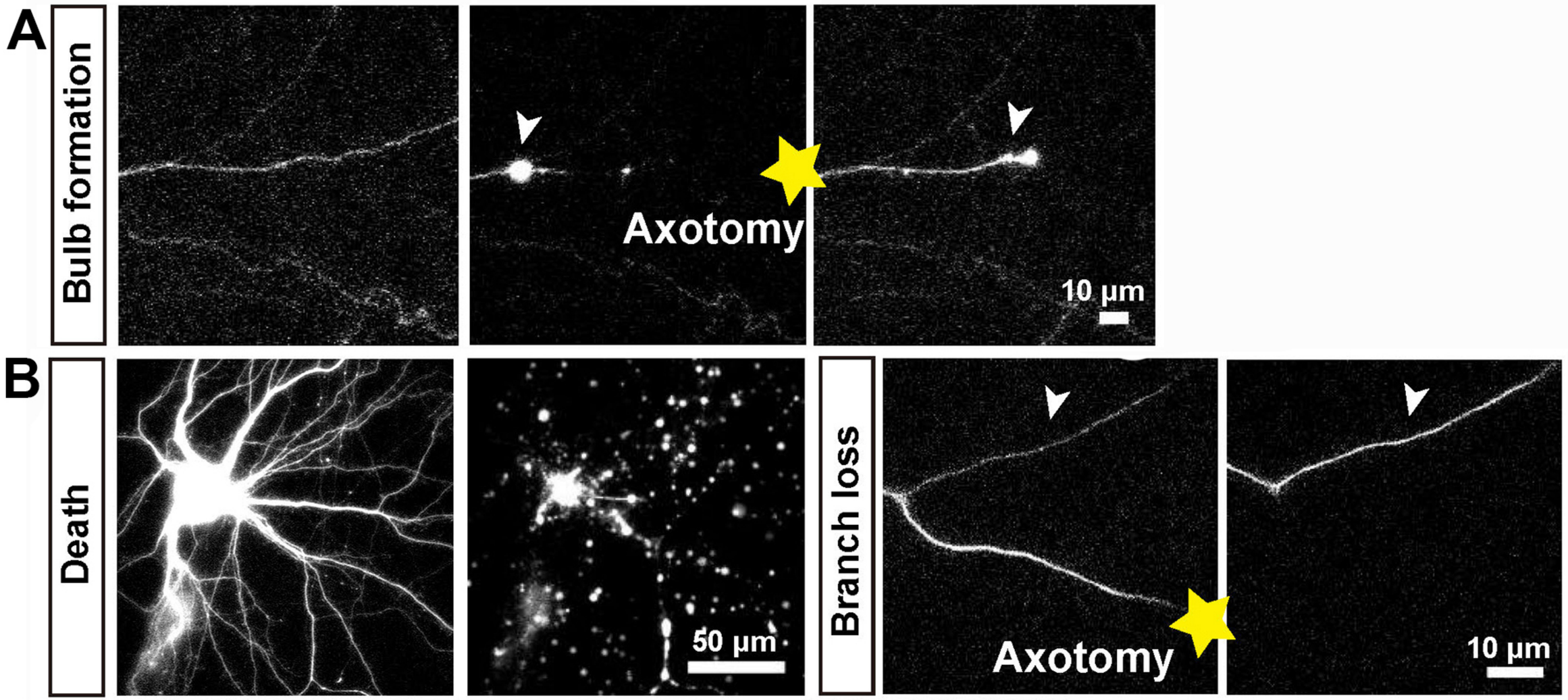
A
Bulb formation
Axotomy
10 µm
B
Death
50 µm
Branch loss
Axotomy
10 µm
C
% of axotomized neurons
80
60
40
20
0
4 DIV n=54
16 DIV n=142
24 DIV n=98
all N.S.
all N.S.
Bulb formation
Branch loss
Death

Figure 2

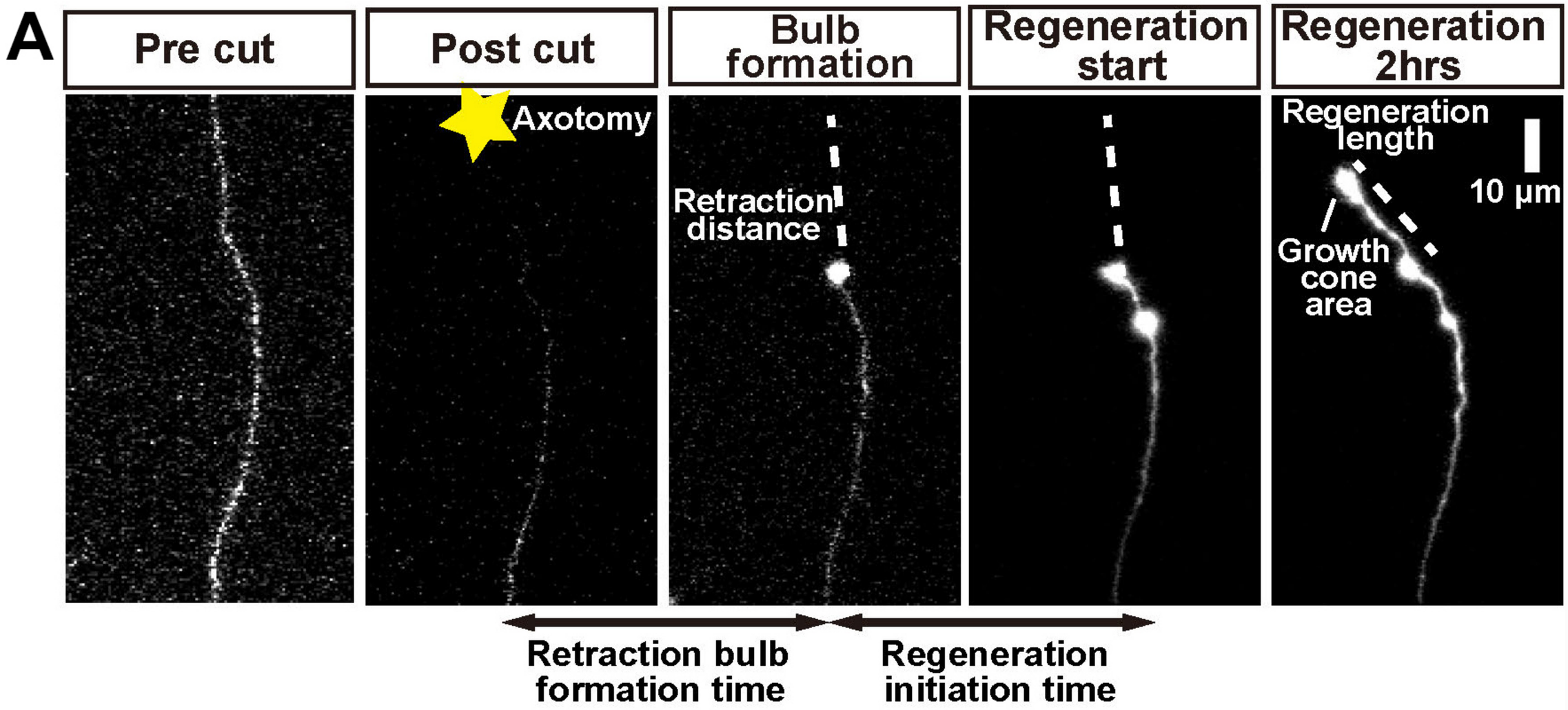
A
Pre cut
Post cut
Bulb formation
Regeneration start
Regeneration 2hrs
Axotomy
Retraction distance
Regeneration length
10 µm
Growth cone area
Retraction bulb formation time
Regeneration initiation time
B
Regeneration
Ectopic growth
Axotomy
10 µm
C
stump formation
ectopic growth
regeneration
n=
35
102
68
axotomy outcome at 10hrs (%)
100
80
60
40
20
0
*
****
****
4 DIV
16 DIV
24 DIV

Figure 3

Retraction → **Growth cone formation**

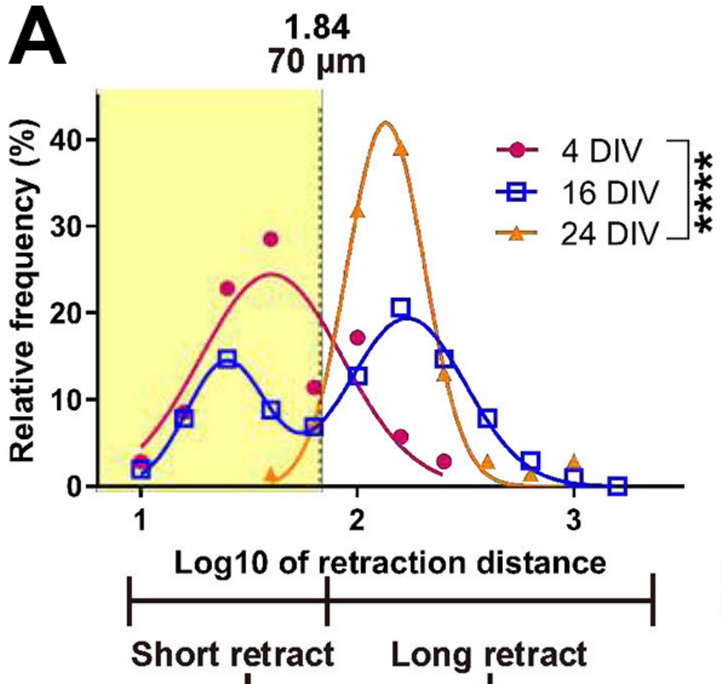

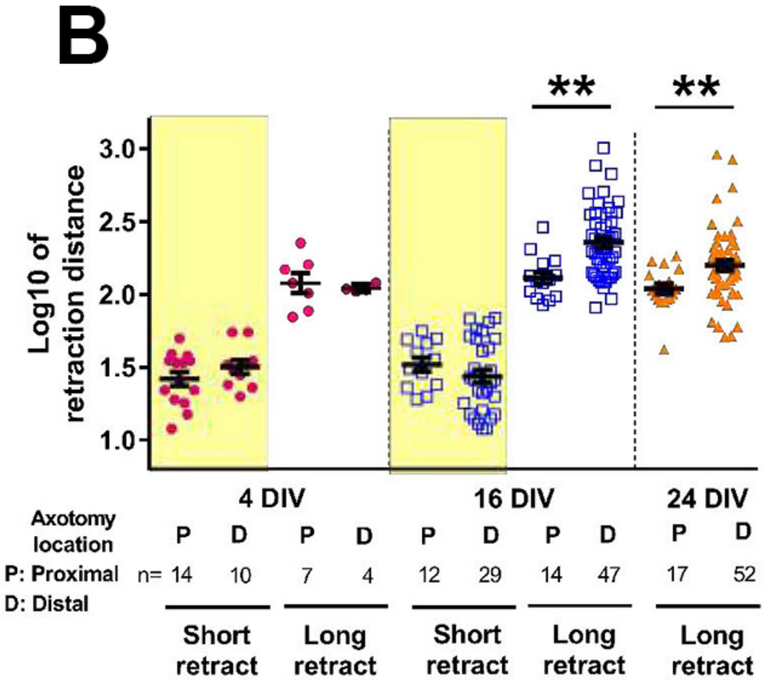

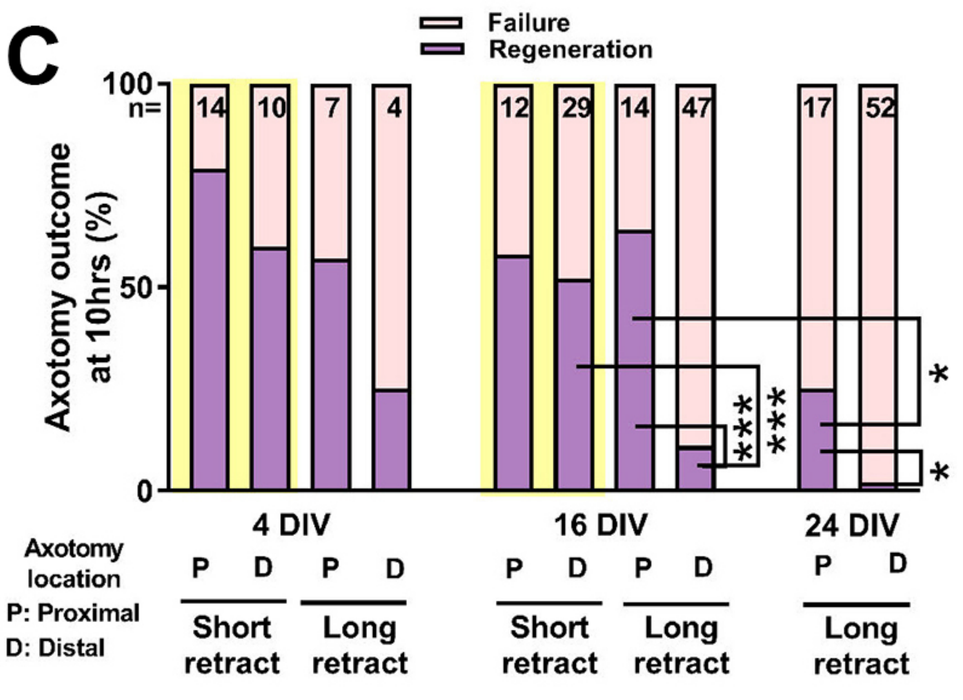

Elongation

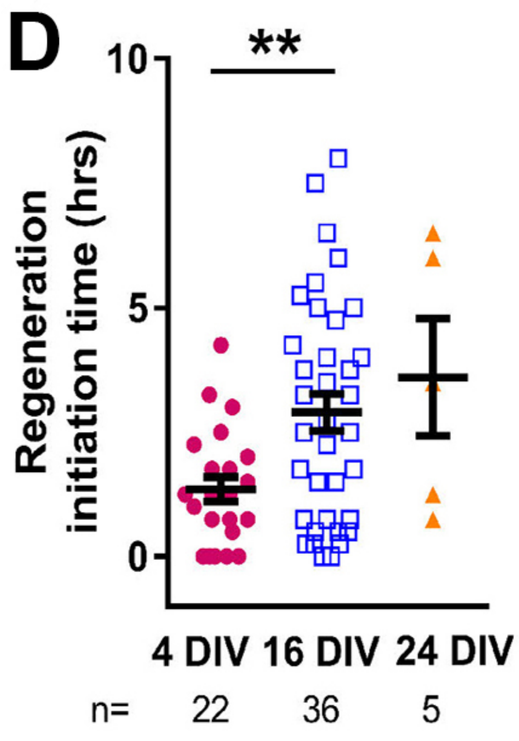

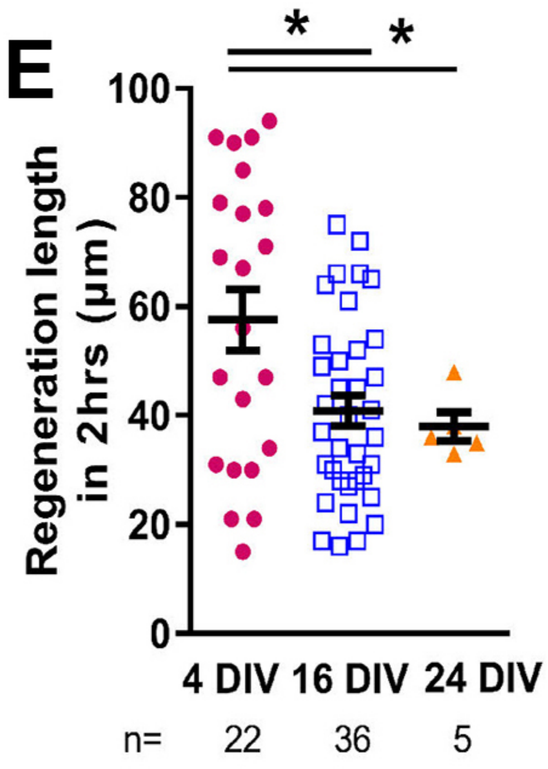

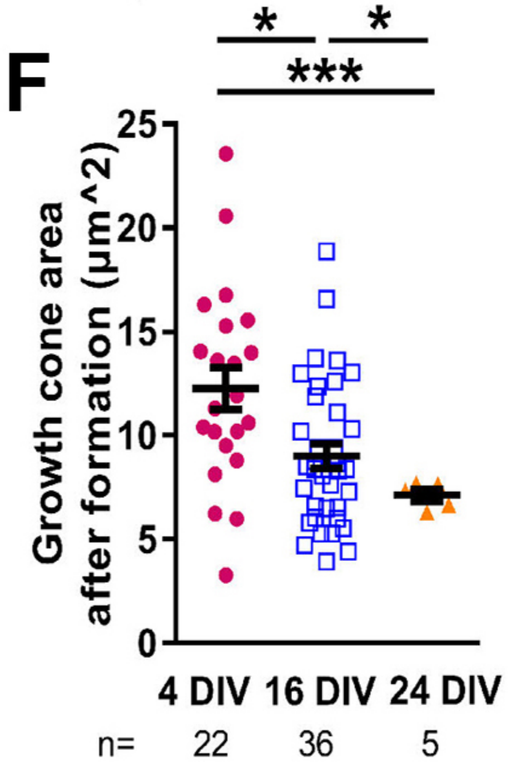

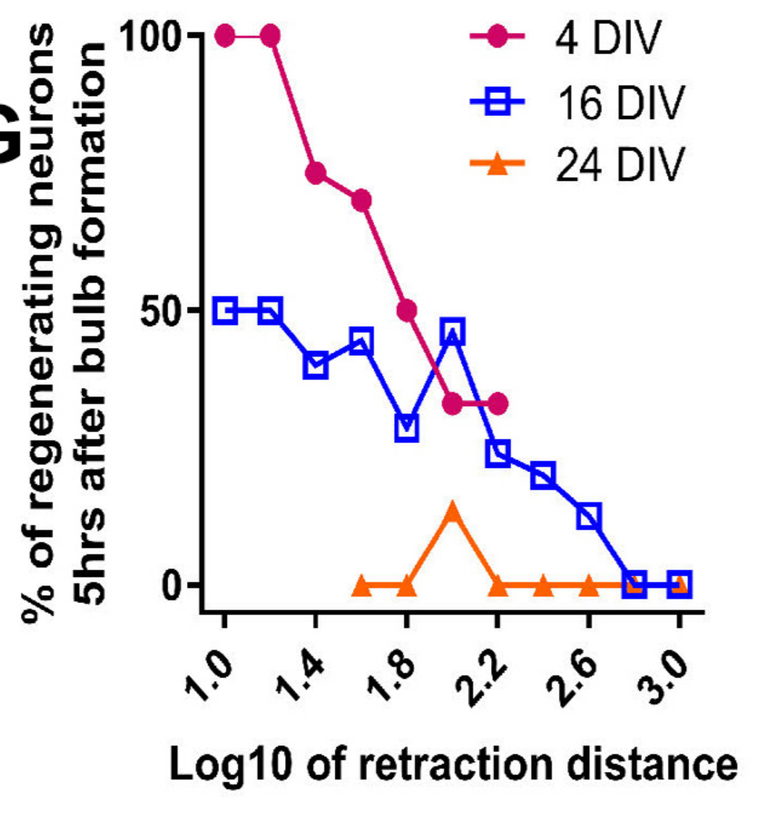

Figure 4

Retraction

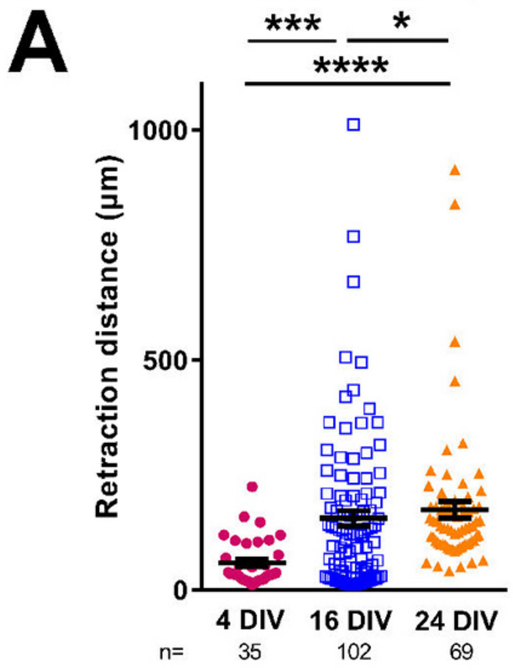

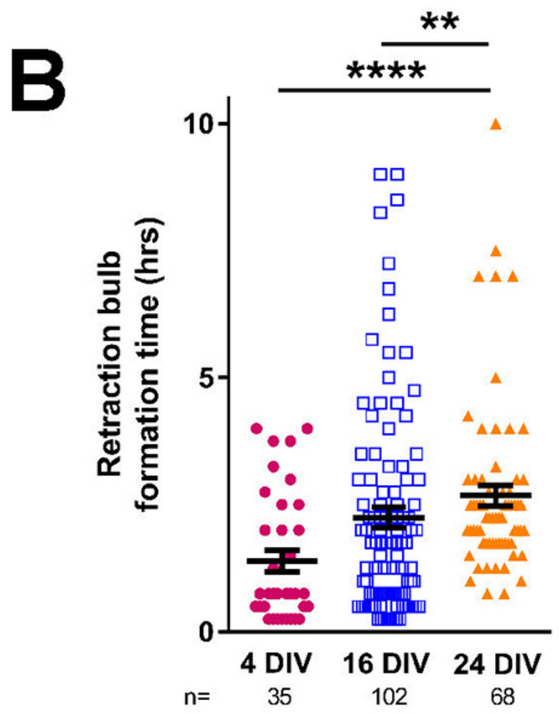

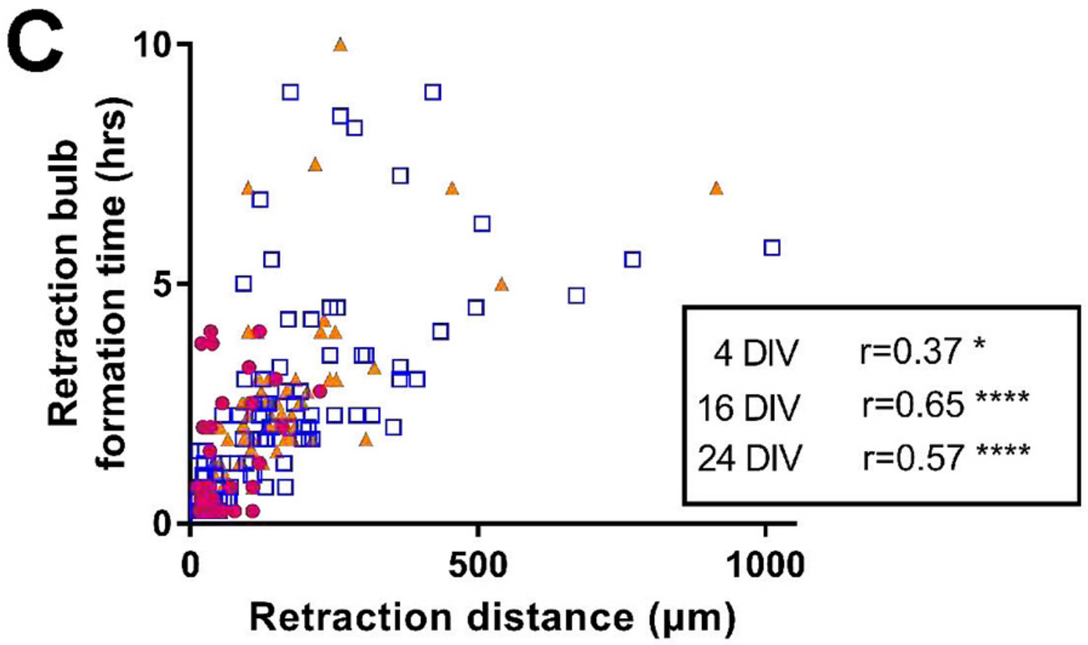

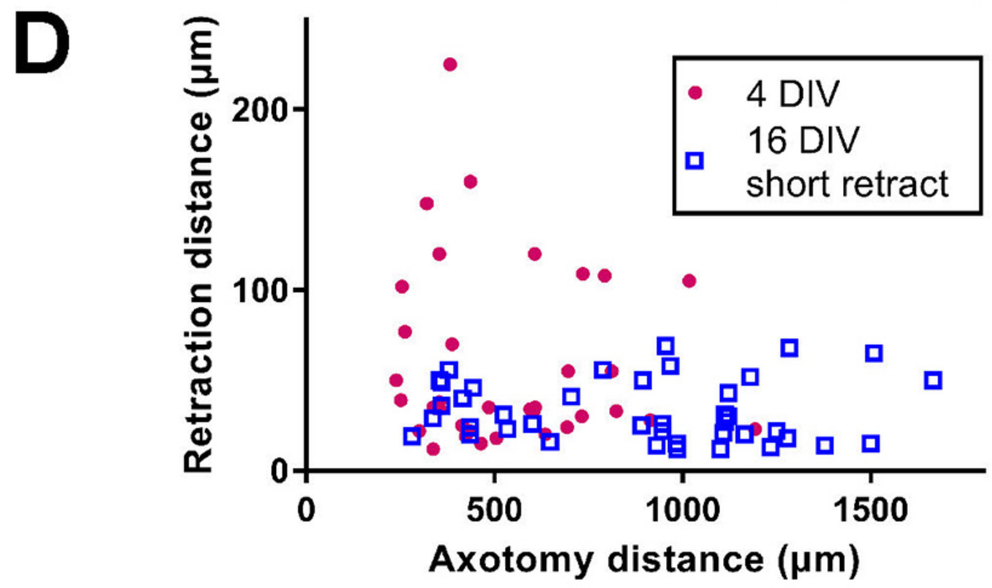

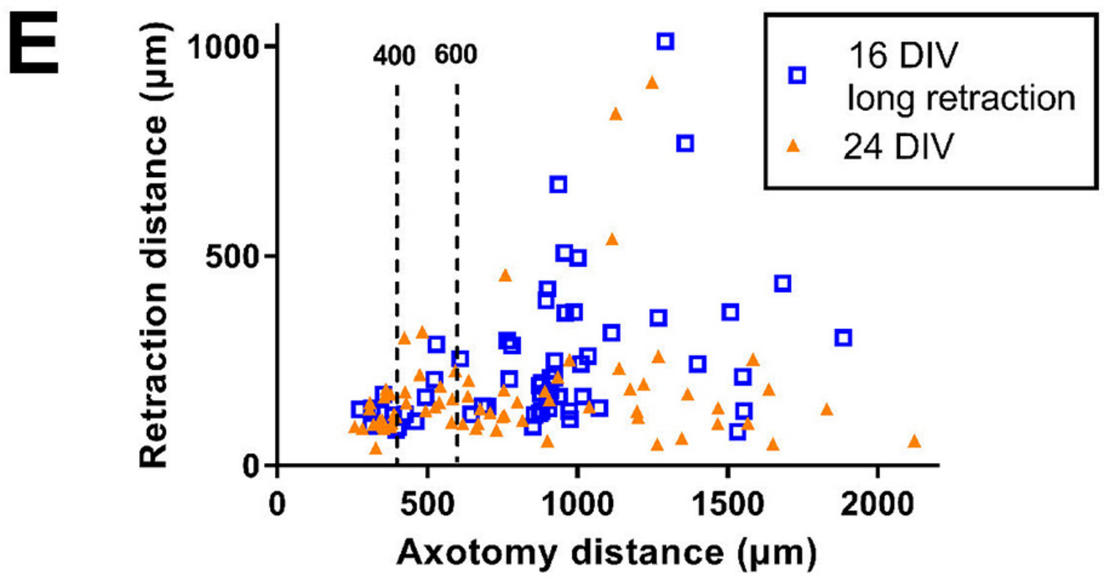

Elongation

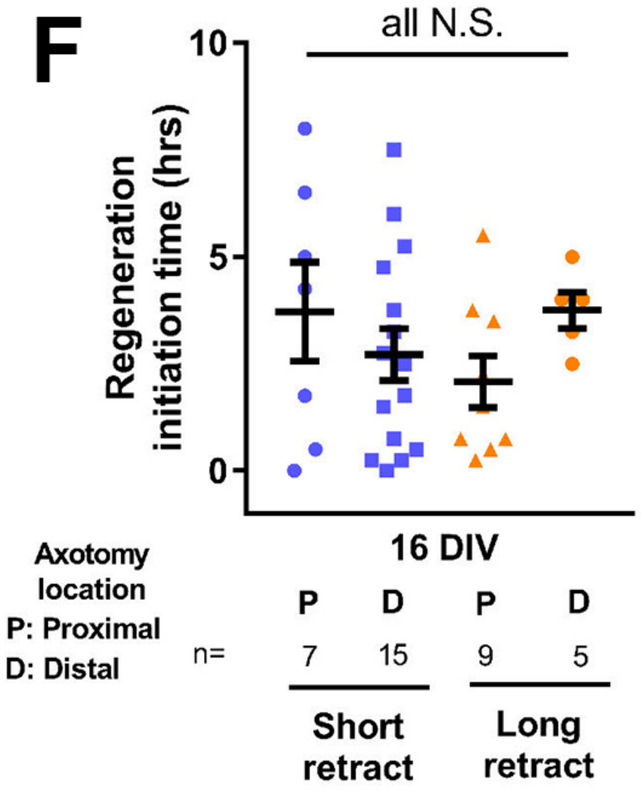

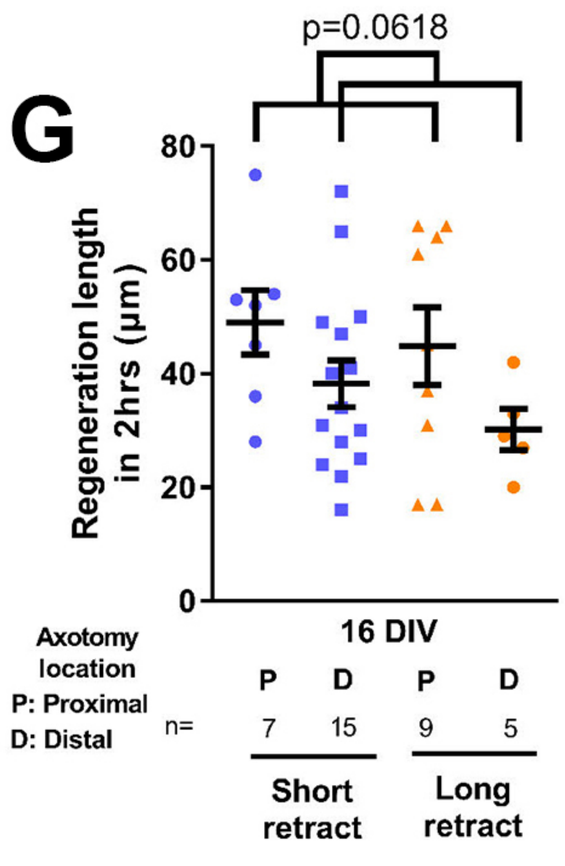

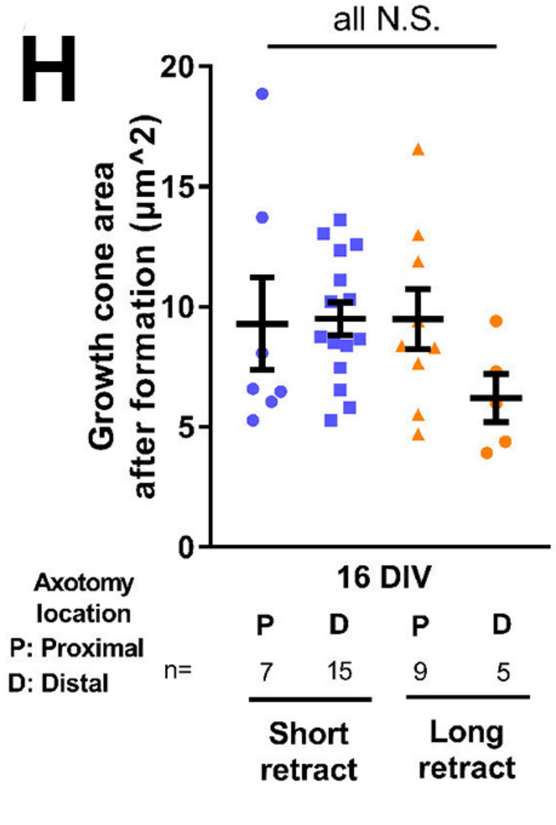

Figure 4 supplementary figure 1

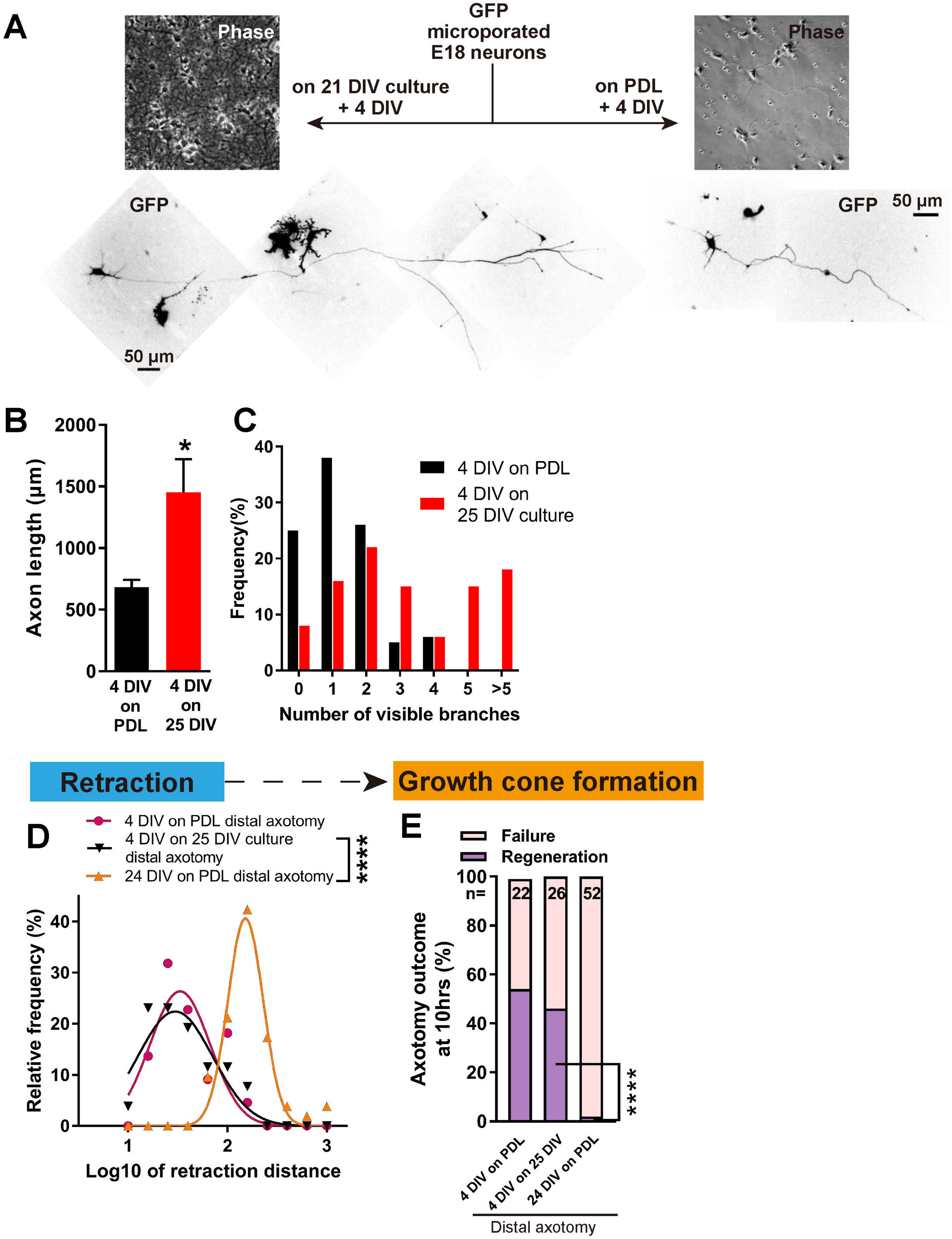
A
Phase
GFP
microporated
E18 neurons
on 21 DIV culture
+ 4 DIV
on PDL
+ 4 DIV
Phase
GFP
50 µm
GFP
50 µm
B
Axon length (µm)
2000
1500
1000
500
0
*
4 DIV on PDL
4 DIV on 25 DIV
C
Frequency(%)
40
30
20
10
0
4 DIV on PDL
4 DIV on
25 DIV culture
0 1 2 3 4 5 >5
Number of visible branches
Retraction
Growth cone formation
D
4 DIV on PDL distal axotomy
4 DIV on 25 DIV culture
distal axotomy
24 DIV on PDL distal axotomy
****
Relative frequency (%)
40
30
20
10
0
1
2
3
Log10 of retraction distance
E
Failure
Regeneration
Axotomy outcome
at 10hrs (%)
100
80
60
40
20
0
n=
22
26
52
****
4 DIV on PDL
4 DIV on 25 DIV
24 DIV on PDL
Distal axotomy

Figure 5

Endogenous

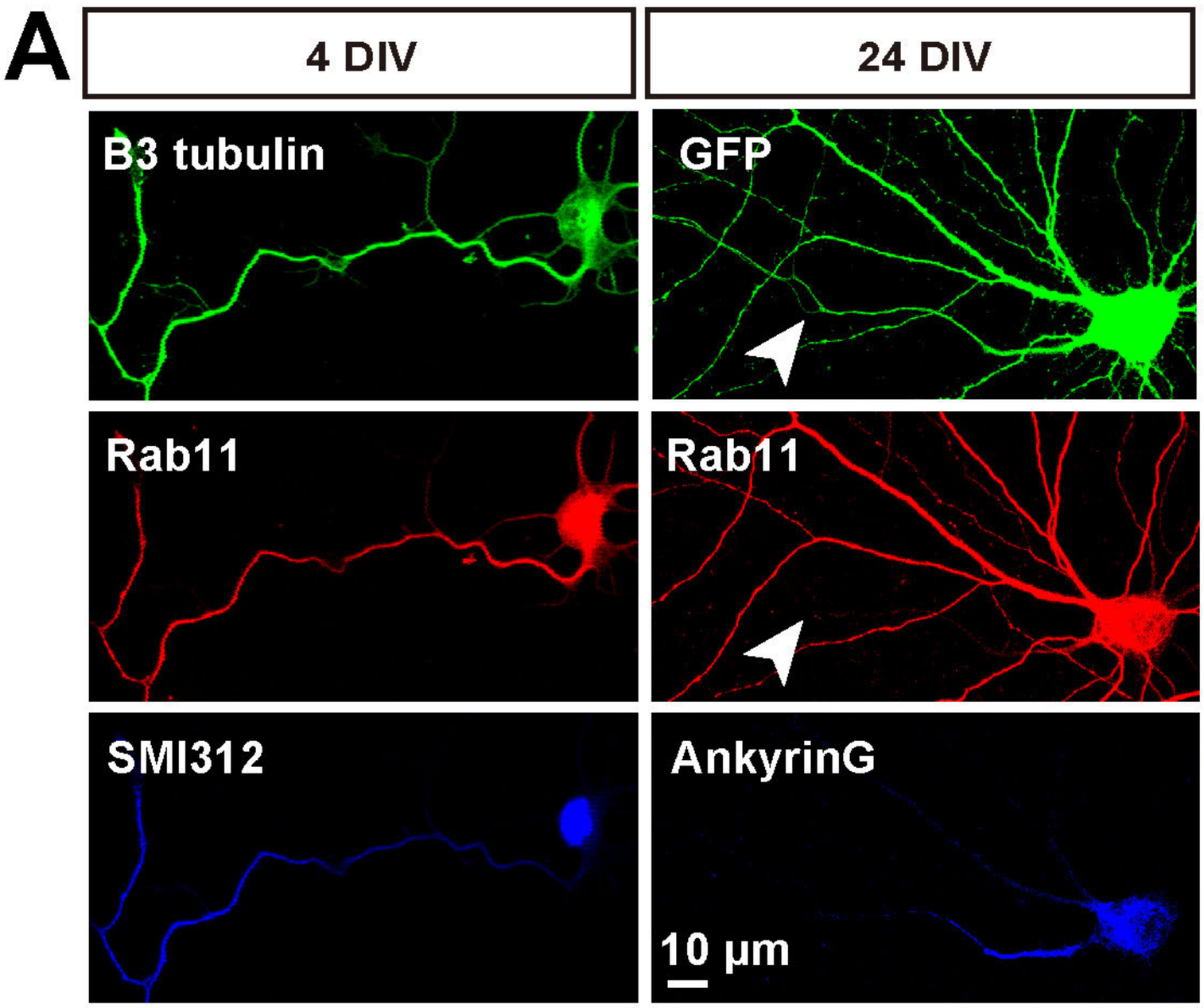

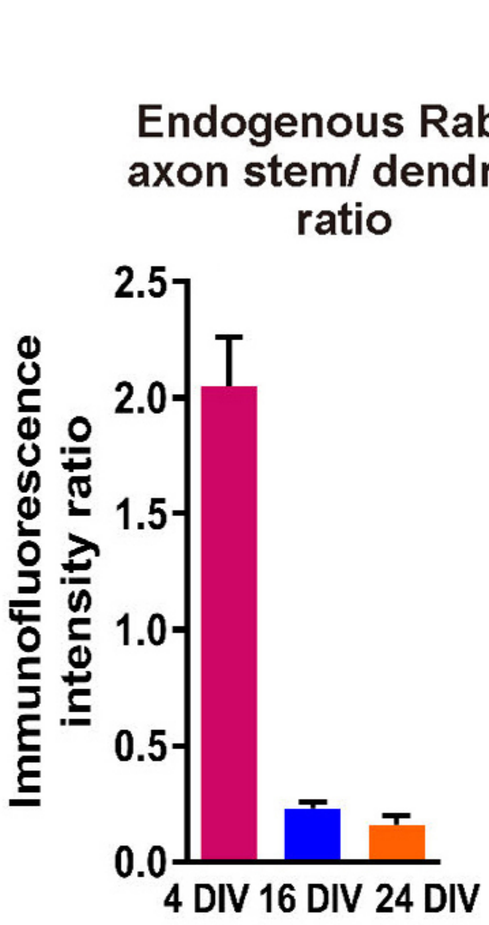

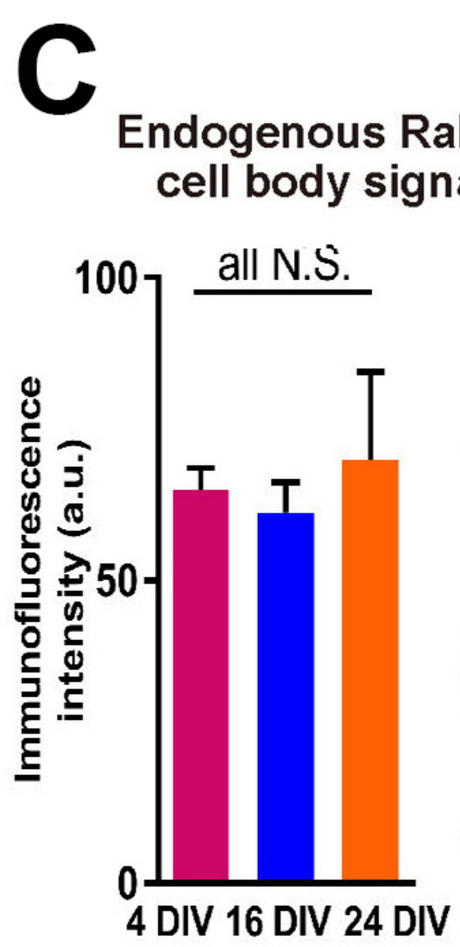

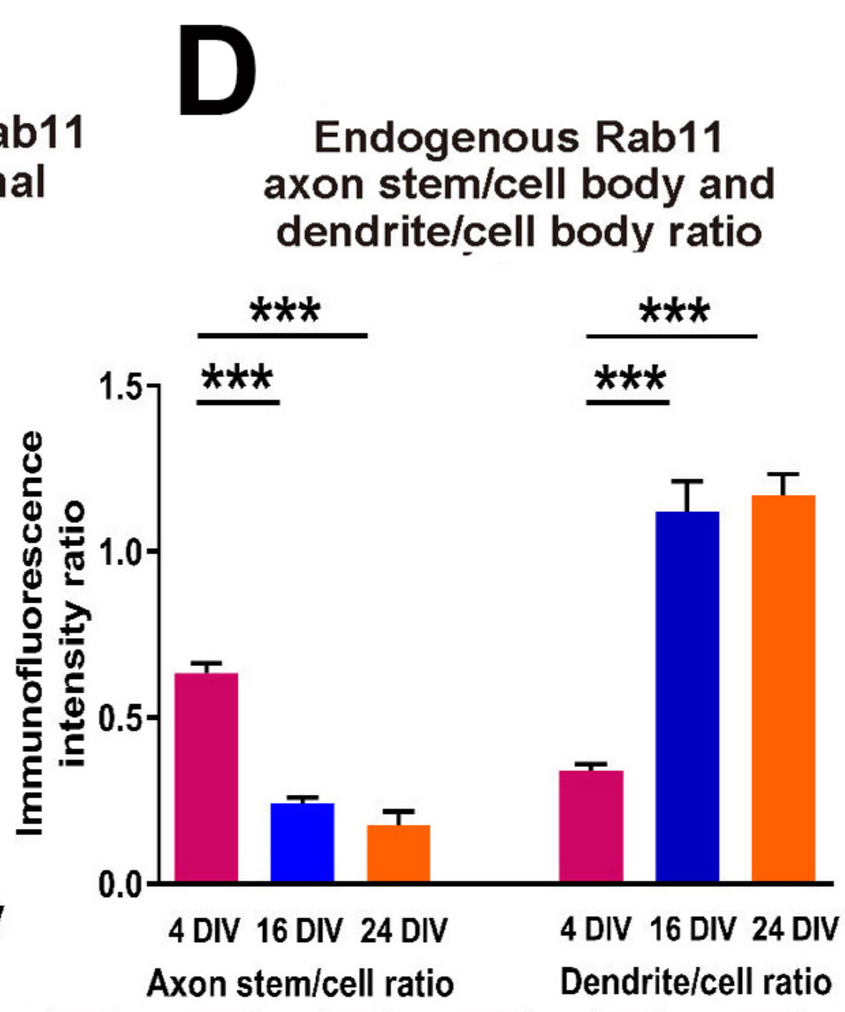

Figure 6

Rab11 overexpression

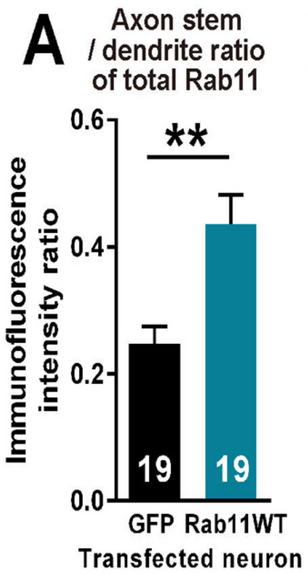

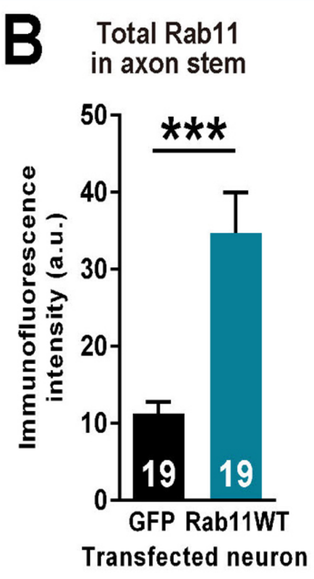

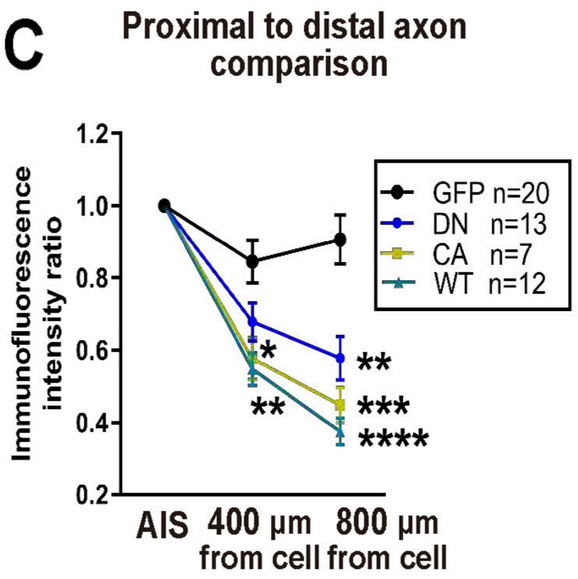

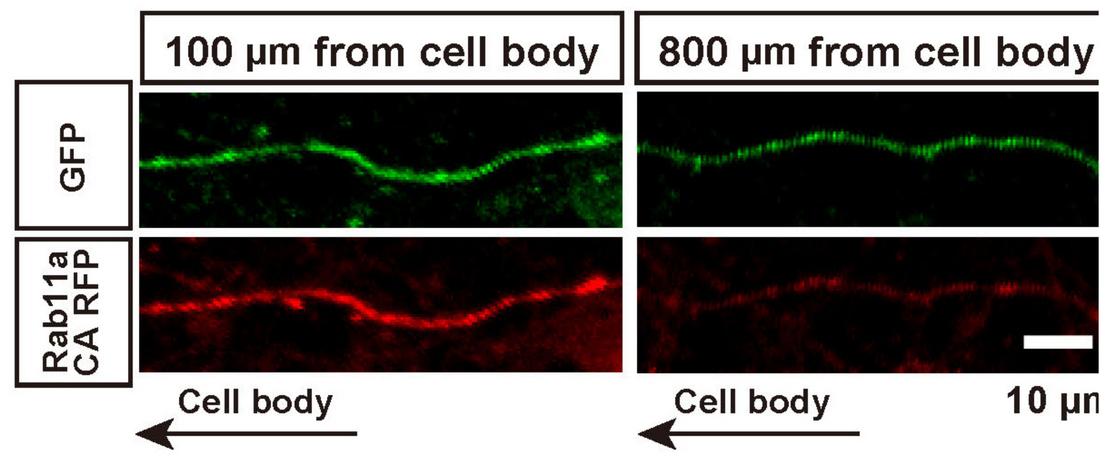

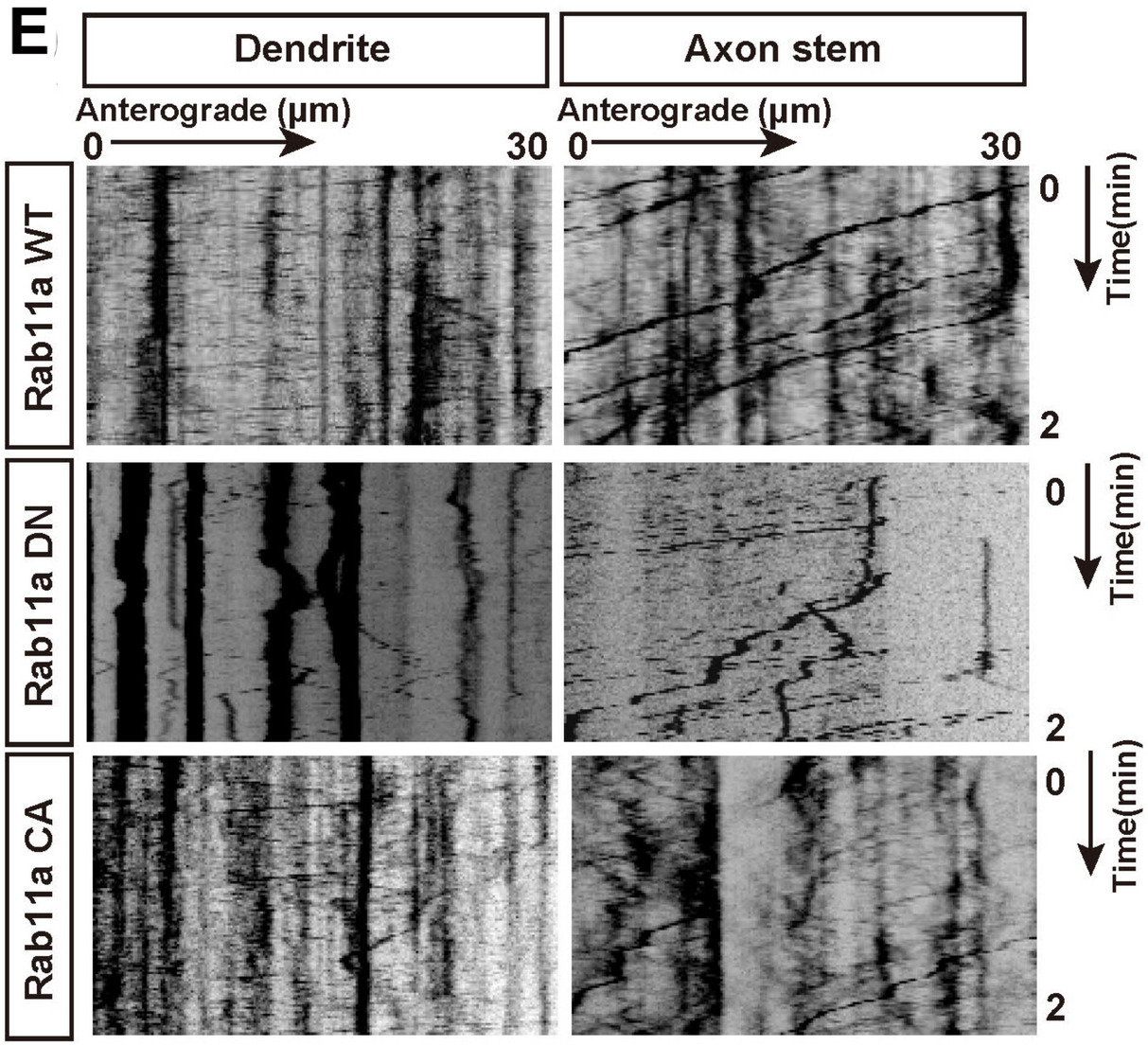

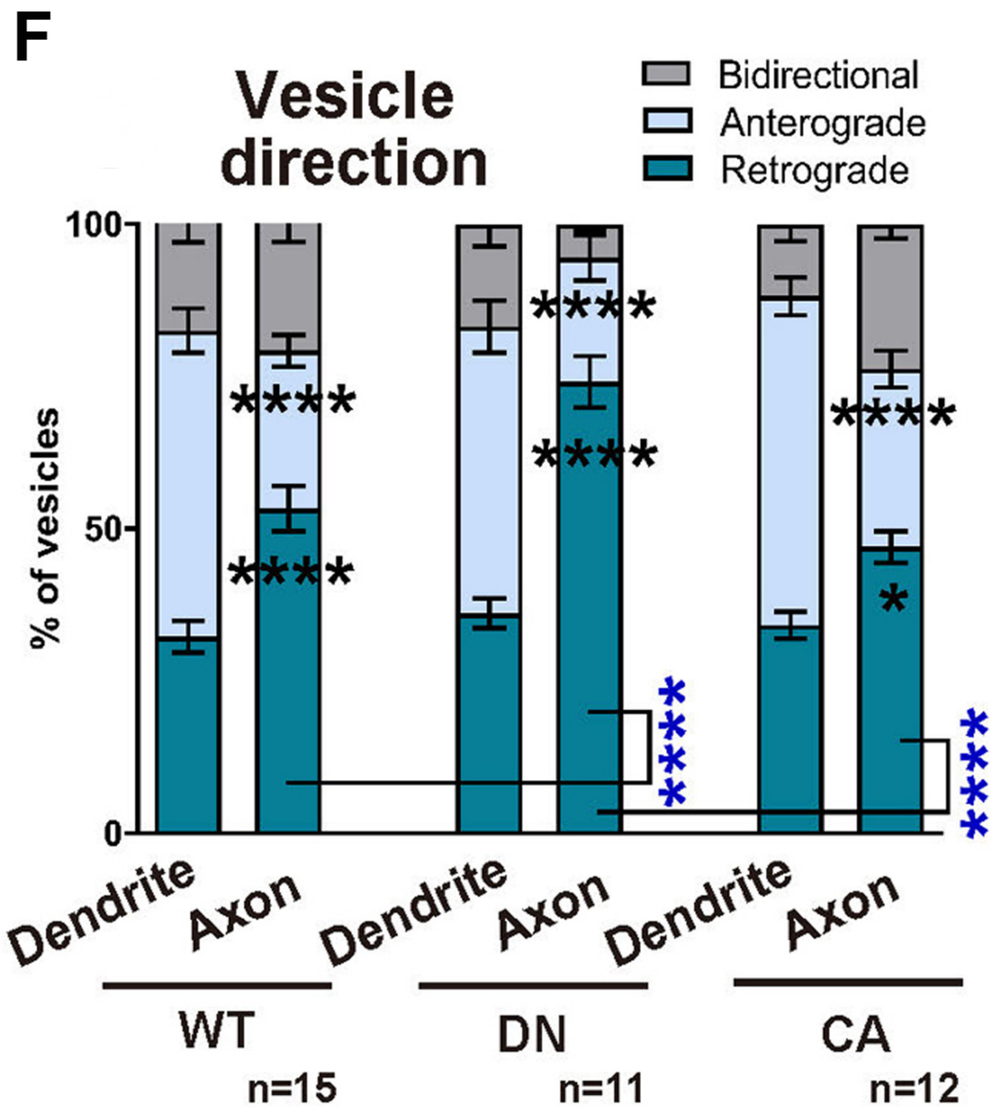

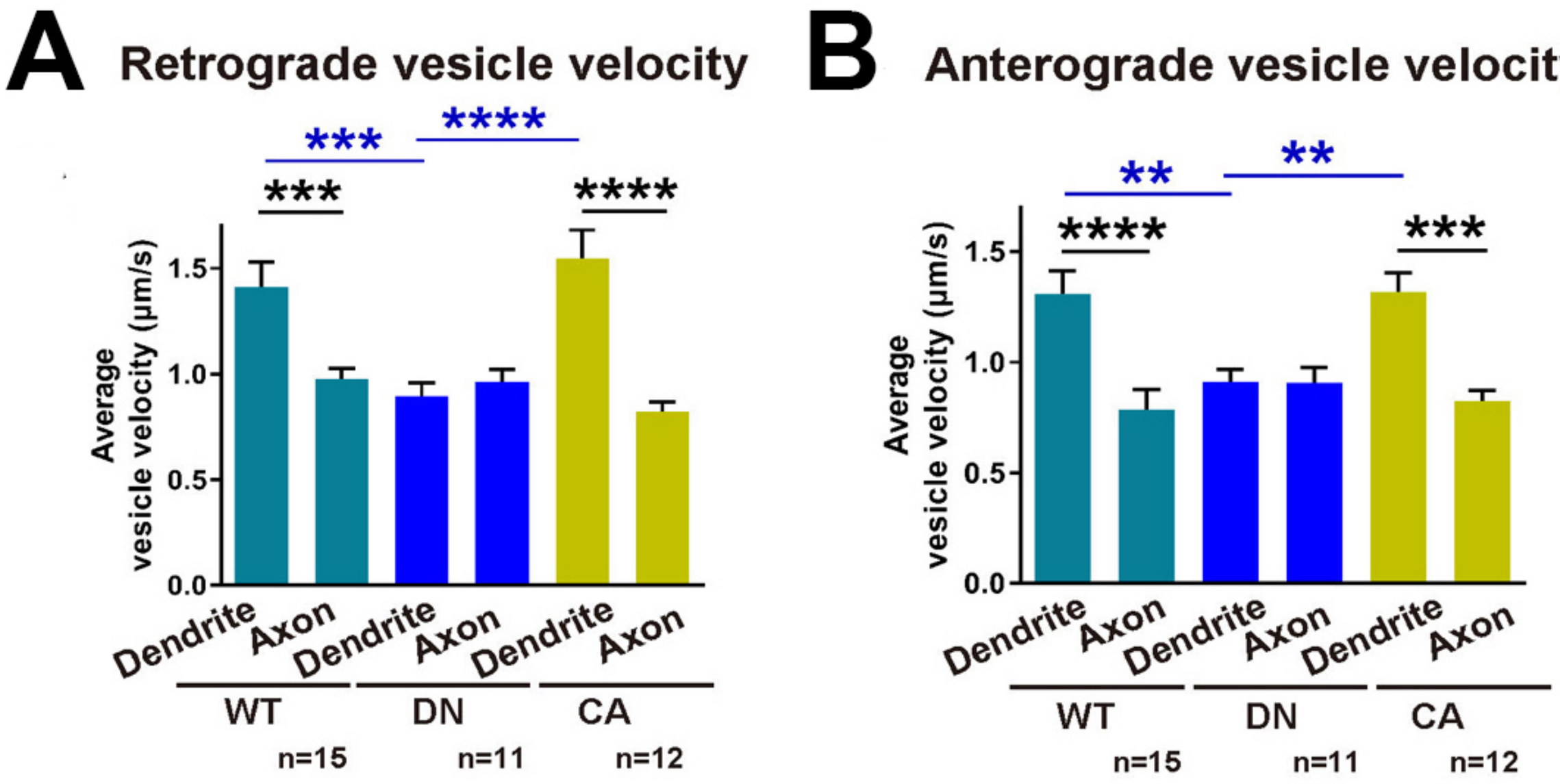

Figure 7 supplementary figure 1

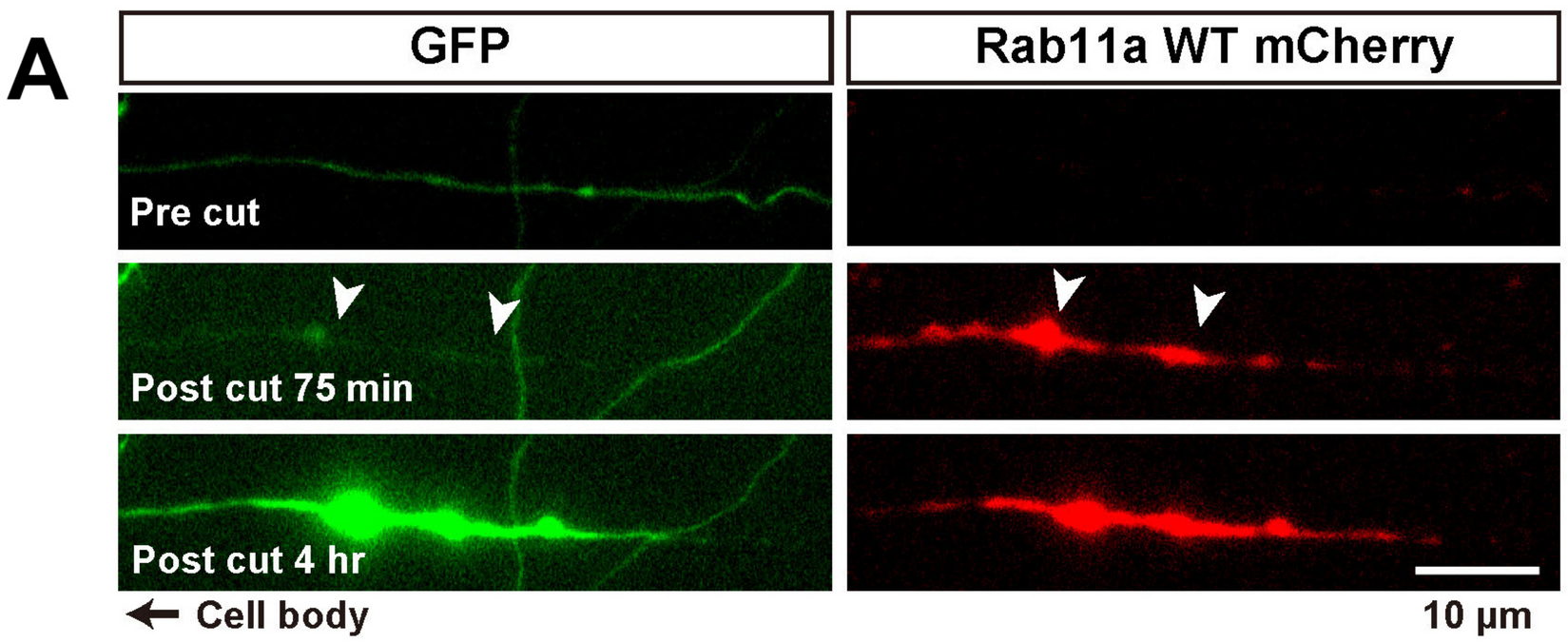
A
GFP
Rab11a WT mCherry
Pre cut
Post cut 75 min
Post cut 4 hr
Cell body
10 µm

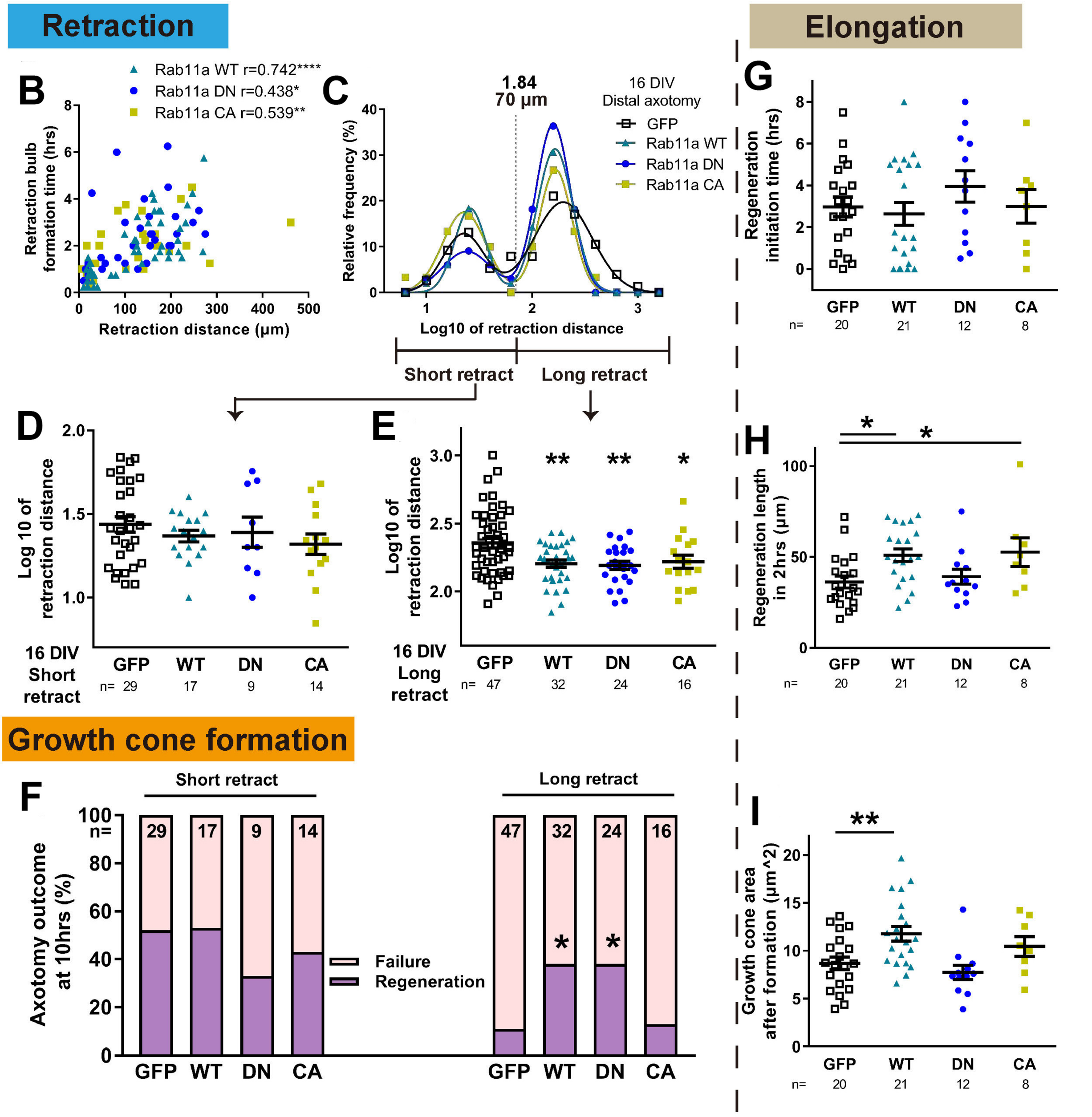
Retraction
Elongation
B
Rab11a WT r=0.742****
Rab11a DN r=0.438*
Rab11a CA r=0.539**
Retraction bulb formation time (hrs)
Retraction distance (µm)
C
1.84
70 µm
16 DIV
Distal axotomy
GFP
Rab11a WT
Rab11a DN
Rab11a CA
Relative frequency (%)
Log10 of retraction distance
Short retract
Long retract
G
Regeneration initiation time (hrs)
GFP WT DN CA
n= 20 21 12 8
D
Log 10 of retraction distance
16 DIV Short retract
GFP WT DN CA
n= 29 17 9 14
E
Log10 of retraction distance
16 DIV Long retract
GFP WT DN CA
n= 47 32 24 16
H
Regeneration length in 2hrs (µm)
GFP WT DN CA
n= 20 21 12 8
Growth cone formation
F
Short retract
Long retract
Axotomy outcome at 10hrs (%)
n=
29 17 9 14
47 32 24 16
Failure
Regeneration
GFP WT DN CA
I
Growth cone area after formation (µm^2)
GFP WT DN CA
n= 20 21 12 8

Figure 8

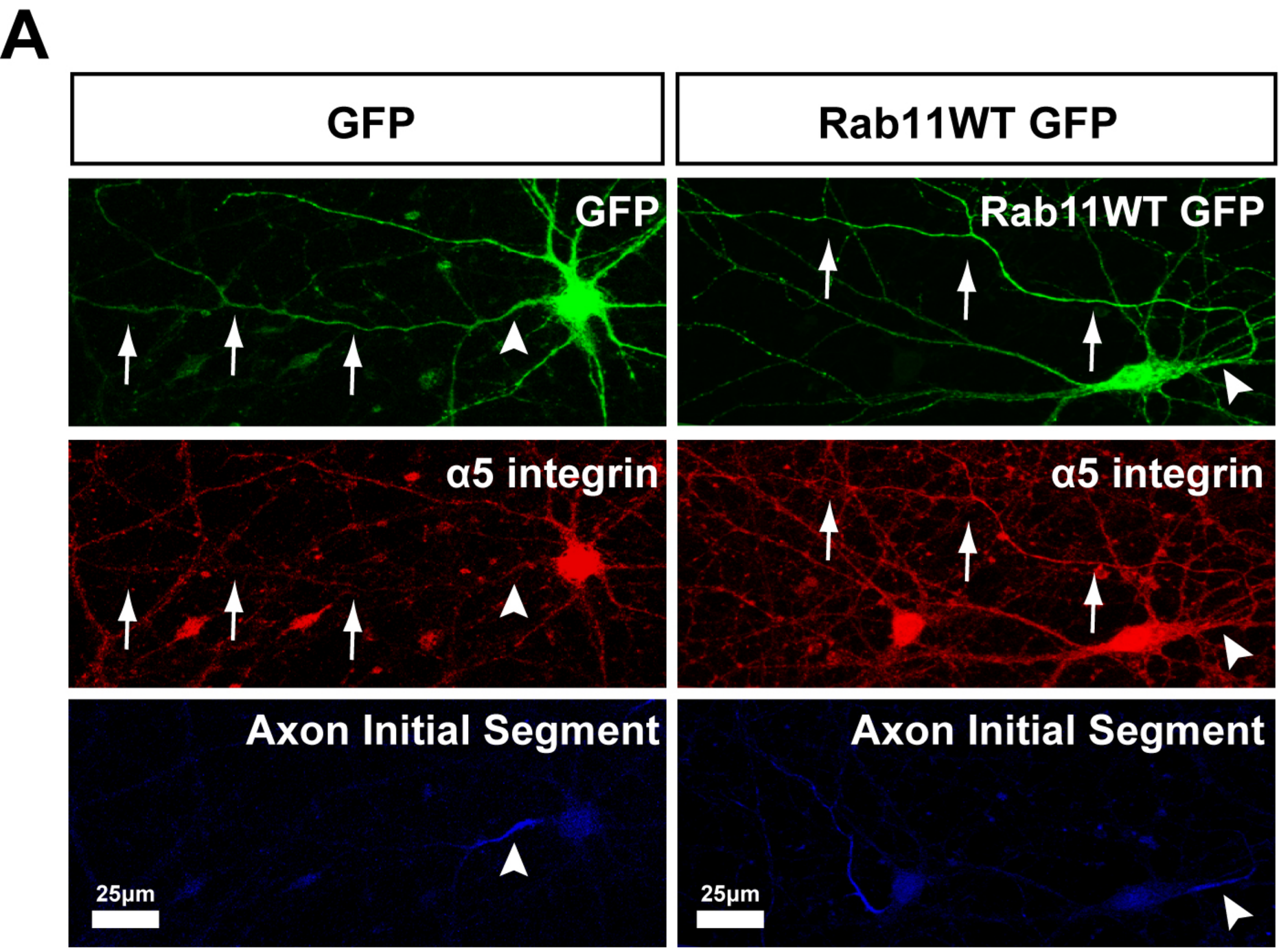
A
GFP
Rab11WT GFP
GFP
Rab11WT GFP
α5 integrin
α5 integrin
Axon Initial Segment
Axon Initial Segment
25μm
25μm

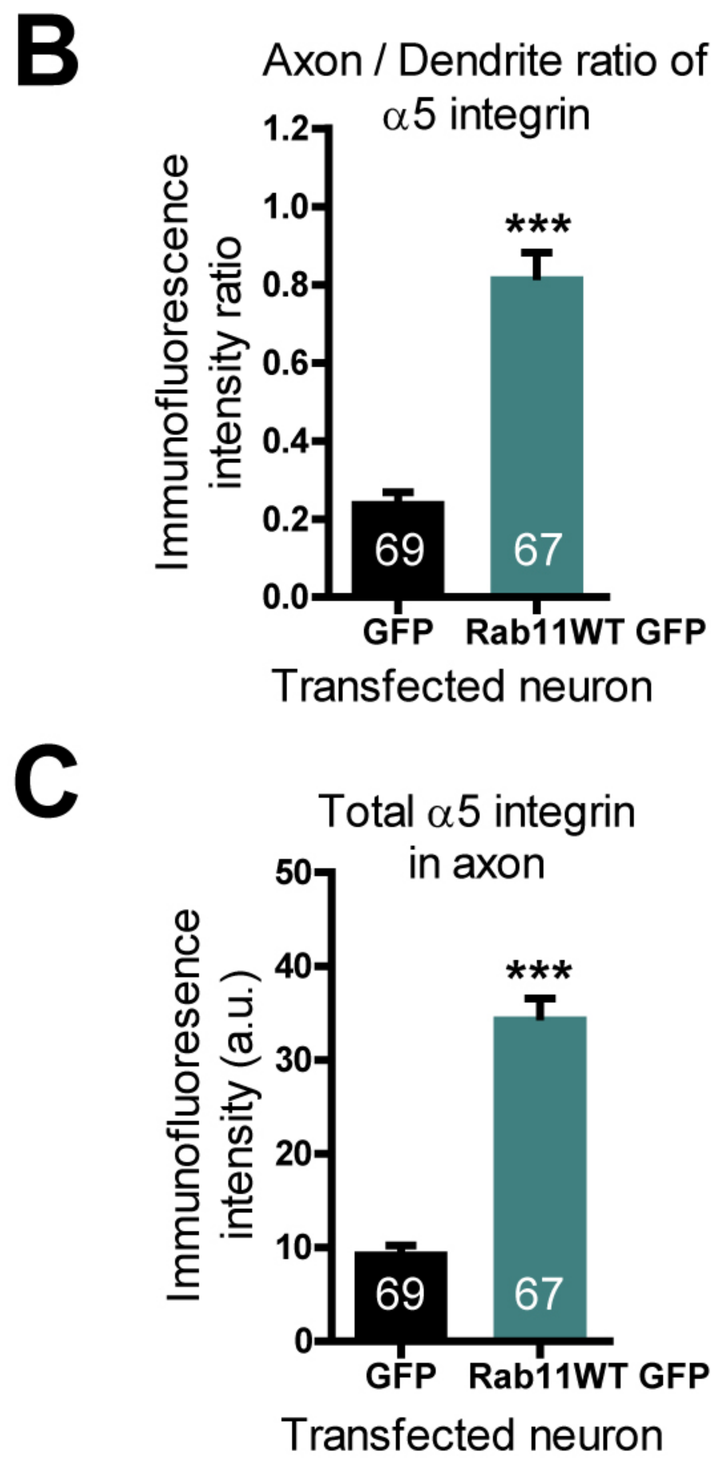
B
Axon / Dendrite ratio of α5 integrin
Immunofluorescence intensity ratio
1.2
1.0
0.8
0.6
0.4
0.2
0.0
***
69
67
GFP
Rab11WT GFP
Transfected neuron
C
Total α5 integrin in axon
Immunofluoresence intensity (a.u.)
50
40
30
20
10
0
***
69
67
GFP
Rab11WT GFP
Transfected neuron

Figure 9

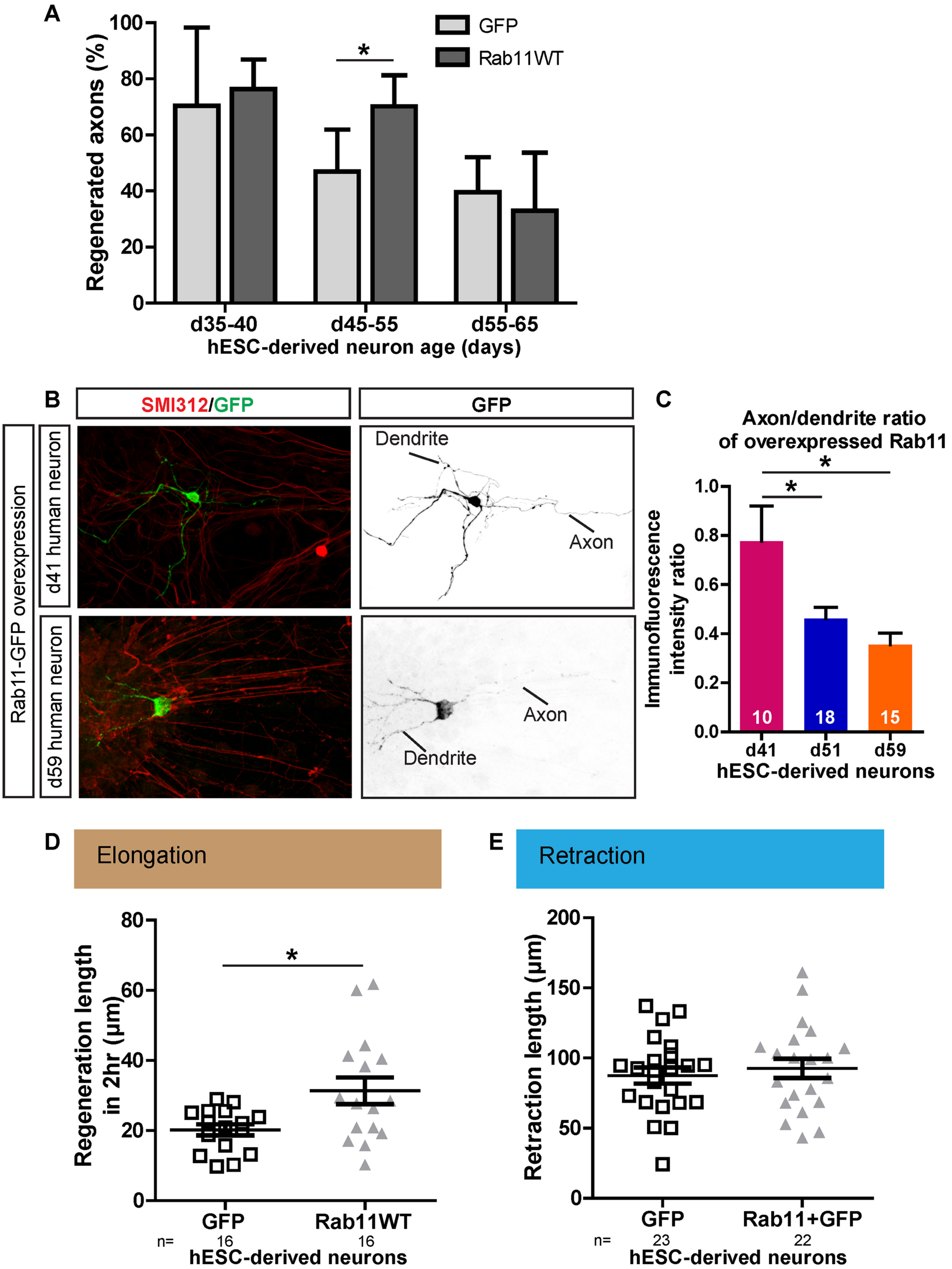
A
Regenerated axons (%)
100
80
60
40
20
0
*
GFP
Rab11WT
d35-40
d45-55
d55-65
hESC-derived neuron age (days)
B
SMI312/GFP
GFP
Rab11-GFP overexpression
d41 human neuron
d59 human neuron
Dendrite
Axon
Dendrite
Axon
C
Axon/dendrite ratio
of overexpressed Rab11
*
*
Immunofluorescence
intensity ratio
1.0
0.8
0.6
0.4
0.2
0.0
10
18
15
d41
d51
d59
hESC-derived neurons
D
Elongation
Regeneration length
in 2hr (µm)
80
60
40
20
0
*
GFP
Rab11WT
n=
16
16
hESC-derived neurons
E
Retraction
Retraction length (µm)
200
150
100
50
0
GFP
Rab11+GFP
n=
23
22
hESC-derived neurons

Figure 10